Complexity in wetting dynamics

Matthieu Roché, Laurence Talini, Emilie Verneuil

Complexity in wetting dynamics

Matthieu Roché,[†,‡] Laurence Talini,[*,¶] and Emilie Verneuil[§]

†*Matière et Systèmes Complexes, Université Paris Cité, CNRS UMR 7057, Paris F-75013*

‡*Department of Materials Physics, Research School of Physics, Australian National University, Australia*

¶*CNRS, Surface du Verre et Interfaces, Saint-Gobain, 93300 Aubervilliers, France*

§*CNRS Sciences et Ingénierie de la Matière Molle, ESPCI Paris, PSL Research University, Sorbonne Université, Paris, France*

E-mail: laurence.talini@cnrs.fr

Abstract

The spreading dynamics of a droplet of pure liquid deposited on a rigid, non-soluble substrate has been extensively investigated. In a purely hydrodynamic description, the dynamics of the contact line is determined by a balance between the energy associated with the capillary driving force and the energy dissipated by the viscous shear in the liquid. This balance is expressed by the Cox-Voinov law, which relates the spreading velocity to the contact angle. More recently, complex situations have been examined in which dissipation and/or the driving force may be strongly modified, leading to sometimes spectacular changes in wetting dynamics. We review recent examples of effects at the origin of deviations from the hydrodynamic model, which may involve physical or chemical modifications of the substrate or of the wetting liquid, occurring at scales ranging from the molecular to the mesoscopic.

1 Introduction

The seemingly straightforward scenario in which a droplet spreads on a solid substrate still challenges engineers and scientists after decades of studies. Because the scales involved range from the molecular level at the contact line to the scale of the droplet itself, this problem encompasses a range of complexities that demand intricate descriptions and meticulous experimentation. The simplest theoretical description of the dynamics of wetting, known as the Cox-Voinov law, balances the work of the driving capillary force induced by the deformation of the liquid/gas interface away from its equilibrium shape and the energy lost by viscous dissipation in the droplet. This law is a crucial tool in the study of wetting since its successes and failures show how the wetting dynamics depends not only on hydrodynamics but also on the physico-chemistry at play at the contact line. The rich literature documenting both experimental and theoretical studies with the aim of gaining a deeper understanding of these issues over the last fifty years is reviewed in numerous works, notably in.[1–3]

A reason for the sustained interest in wetting dynamics lies in the exploration of more complex situations, beyond that of a pure liquid wetting a rigid substrate. In addition to their fundamental interest, complex conditions are often encountered in industrial applications. For instance, in the wet coating process widely used in industry, complex fluids generally containing solutes or suspended particles are needed to form a continuous film on a substrate at the highest possible speed. The characteristic length and time scales of the fluid can lead to wetting behaviours that significantly depart from purely hydrodynamic phenomena. In other applications, coatings are applied to control the wetting properties of surfaces. As an example, hydrogel layers are used as anti-fogging coatings because they promote the formation of a condensed water film instead of droplets, which alter optical properties.[4,5] This involves the wetting of a simple liquid on a poroelastic and deformable coating. A description of wetting in these conditions has yet to be proposed.

The present review focuses on the experimental aspects of the recent literature on wetting dynamics, with a particular emphasis on the effects related to the physico-chemistry of

the systems under consideration. We begin with the hydrodynamic description of wetting dynamics for simple liquids and solids, and then illustrate by providing a non-exhaustive set of examples how this dynamics can deviate from the Cox-Voinov law when a higher degree of complexity in the system is considered.

The text is organised as follows: In Section 2, we recall how the Cox-Voinov law is established. Then we review some effects that modify either the driving capillary force or the nature of the dissipative process, namely: line friction and retardation mechanisms in Section 3, dissipation in the substrate in Section 4, surfactant-induced Marangoni effects in Section 5. The last section deals with finite-size effects.

2 Hydrodynamic model

We recall here the basic principles underlying the hydrodynamic model describing the relation between the shape of the interface of the droplet in the vicinity of the contact line and its velocity. Our aim is not to provide a thorough discussion of the physics at play in this region. We suggest that the reader refers to past reviews[1,3,6] for more details.

We consider a droplet of liquid of density ρ, viscosity η and surface tension γ placed on a solid substrate. We denote respectively as γ_{sv} and γ_{sl} the surface energies of the solid with air and with the liquid. The droplet is in equilibrium when its contact angle, defined as the angle of the contact line with the solid substrate measured inside the droplet (see figure 1), has the equilibrium value θ_e. In partial wetting conditions, $\gamma_{sv} - \gamma_{sl} < \gamma$, and θ_e has a finite value given by the balance of the horizontal forces per unit length acting on the contact line, given by the the Young-Dupré law,

$$\cos\theta_e = \frac{\gamma_{sv} - \gamma_{sl}}{\gamma}. \tag{1}$$

In total wetting conditions, $\gamma_{sv} - \gamma_{sl} > \gamma$, and the equilibrium angle θ_e is zero. The liquid forms a film with a thickness determined by the inter-molecular forces at stake.

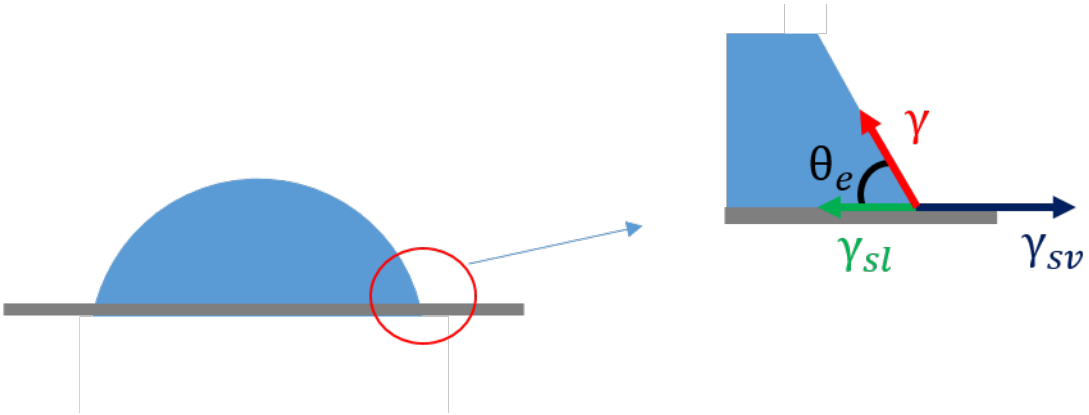

Figure 1: Schematics of a droplet sitting on a solid substrate and of the forces acting on the contact line.

When the contact angle has a value different from its equilibrium one, the contact line is submitted to the capillary force

$$F = \gamma_{sv} - \gamma_{sl} - \gamma cos\theta = \gamma(cos\theta_e - cos\theta) \tag{2}$$

The contact line has then a velocity U, which can be related to the angle θ by considering that the work of the driving capillary force is entirely dissipated by the viscous flow generated in the drop. In the picture suggested by de Gennes,[1] the vicinity of the contact line is assimilated to a wedge in which a Poiseuille flow takes place, as shown in figure 2, with average velocity equal to U. In this simplified view, the wedge height h at a distance x to the contact line is given by $h = \theta x$. More refined derivations accounting for the curvature of the air liquid interface are not detailed here but ascribed the Poiseuille flow to the gradient of capillary pressure resulting from curvature effects.

If a zero velocity boundary condition at the substrate is assumed, the shear stress scales as $\eta U/h$. Viscous stresses at the contact line should then diverge and prevent the motion of the contact line, in opposition with our everyday experience. This paradox, identified by Huh and Scriven[7], is solved by considering that effects allowing the line to slide on the solid surface are at play below a characteristic microscopic distance to the contact line, ℓ. In this frame, the power dissipated by the viscous flow is computed at distances larger than the

cut-off length ℓ

$$P_{vis} = \int_{\ell}^{x} dx' \int_{0}^{h} \eta \left(\frac{dv}{dz}\right)^2 dz \tag{3}$$

with the notations defined in Fig. 2 and where v is the velocity field having a mean value equal to the contact line velocity U, and x the distance to the contact line at which the angle θ is measured.

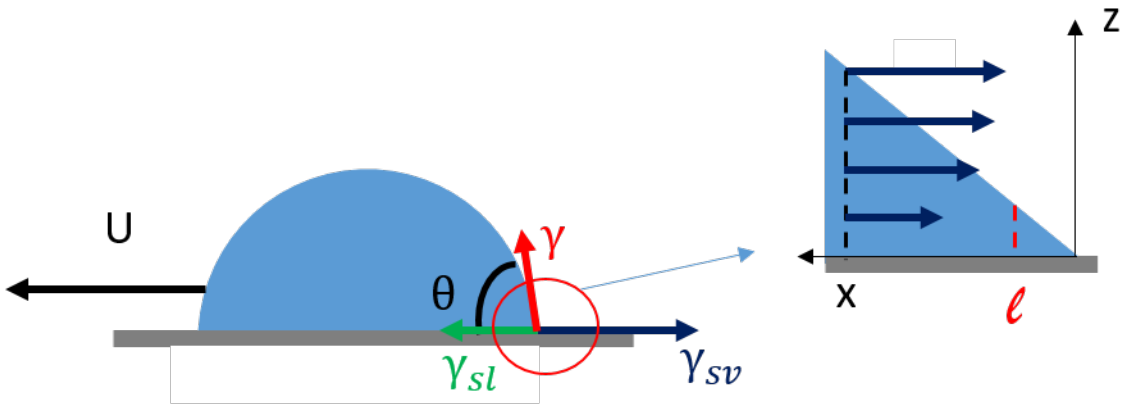

Figure 2: Schematized view of a drop spreading on a solid substrate and of the lubrication flow in the vicinity of the contact line, which is assimilated to a wedge with angle θ.

Since $\frac{dv}{dz} \propto \frac{U}{h}$ with the wedge height varying as $h = \theta x'$ with the distance x' to the contact line, the expected scaling for the dissipated power is $P_{vis} \propto \eta U^2 \theta ln\left(\frac{x}{\ell}\right)$. In the limit of small angles, the power of the driving force is $P_{cap} \simeq \gamma U(\theta_e^2 - \theta^2)/2$. The relationship between velocity and contact angle is obtained by equating powers, which yields

$$\theta^3 - \theta_e^3 \propto \frac{\eta U}{\gamma} ln\left(\frac{x}{\ell}\right). \tag{4}$$

The difference of the cubed dynamic and static angles is therefore proportional to the capillary number, $Ca = \eta U/\gamma$, that compares viscous drag to surface tension forces. Increasing capillary numbers, *i.e.* increasing energy dissipation in the liquid, result in increasing differences between the dynamic and the equilibrium angles.

A full resolution of Stokes' equation in the lubrication approximation, made indepen-

dently by Voinov[8] and Cox[9] yields

$$g\left(\theta(x)\right) - g\left(\theta(\ell)\right) = Ca \ln\left(\frac{x}{\ell}\right) \tag{5}$$

where $g\left(\theta\right) = \int_0^\theta \frac{\beta - cos\beta sin\beta}{sin\beta} d\beta$. For angles smaller than $3\pi/4$, the function g can be approximated,[8,10] which yields the relation known as the Cox-Voinov law

$$\theta^3 - \theta_e^3 = 9Ca \ln\left(\frac{x}{\ell}\right) \tag{6}$$

which is close to that given by the scaling analysis (Eq. 4), but remains valid even for large values of the dynamic angle.

Cox has generalised the result to cases in which the droplet is immersed in a viscous liquid instead of air.[9] In this frame, the relation between angle and velocity can be approximated by[11]

$$\theta^a - \theta_e^a = bCa \ln\left(\frac{x}{\ell}\right) \tag{7}$$

where a and b depend on the viscosity ratio of the drop and surrounding liquid.

Equations 6 and 7 are valid at distances to the contact line where capillary prevails over gravity, i.e. smaller than the capillary length, $\ell_c = \sqrt{\gamma/(\rho g)}$, where g is the acceleration of gravity. As a result, the radius variations with time of viscous droplets with radii $R < \ell_c$ can be derived from Eq. 6 . For a zero equilibrium angle, $U = \dot{R} \propto \theta^3$ and conservation of droplet volume imposes that $R^3 \propto \theta^{-1}$ in the limit of small contact angles. As a result, $\dot{R} \propto R^{-9}$ and, finally, we obtain Tanner's law:

$$R \propto t^{\frac{1}{10}}. \tag{8}$$

Here, we emphasize that the exact integration of the differential equation assumes inital conditions (radius R_0 at time zero) so that $R^{10} - R_0^{10} \propto t$. Hence, a simple testing of an exponent from a $R(t)$ log-log plot is only valid if $R >> R_0$, a condition that is not always

fullfilled in experiments. The validity of Tanner's law also requires volume conservation, no gravity, and that the hypotheses underlying the Cox-Voinov law hold. Hence, another power law is obtained when the radius of the droplet becomes larger than ℓ_c. In this case, viscous dissipation balances gravity, and the exponent is $1/8$.[12] These power-laws are valid only some time after deposition of a droplet on a substrate,[13] when dissipation near the contact line dominates the flow. Moreover, while these laws are established under the assumption of complete wetting, $\theta_{eq} = 0$, they may remain valid provided $\theta >> \theta_{eq}$. Finally, the exponent differs if the liquid spreads in 2D rather than 3D[14] due to a modified volume conservation equation. These remarks support the idea that care should be taken when interpreting droplet spreading data in terms of power-laws to make sure that the underlying assumptions are valid in the systems of interest, and that initial and final conditions are correctly accounted for. Other effects, such as inertia, lead to power laws with exponents larger than $1/10$.[15,16]

The simplest test of the Cox-Voinov law consists in the deposition of a droplet on a solid substrate and the measure of the contact angle as a function of the velocity of the contact line during its spontaneous spreading. However, the range of contact angles and velocities is often small. This issue is circumvented by imposing the relative velocity of the contact line with respect to the substrate. Some experimental situations are illustrated in figure 3. Whichever way is chosen to set the contact line in motion, the dynamics at the contact line is governed by the same capillary force as in spontaneous wetting conditions, and the Cox-Voinov law is expected to be valid provided the flow in the drop satisfies the different conditions detailed in the preceding section.

Experimental checks of the Cox-Voinov law are shown in figure 4. The figure is reproduced from the review by Bonn et al.[6] and compiles data obtained by different authors for oils spreading on surfaces in total wetting conditions. The dynamic angle is much larger than the equilibrium contact angle at capillary numbers much smaller than unity. The experimental data shows an excellent agreement with the Cox-Voinov law. The corresponding value

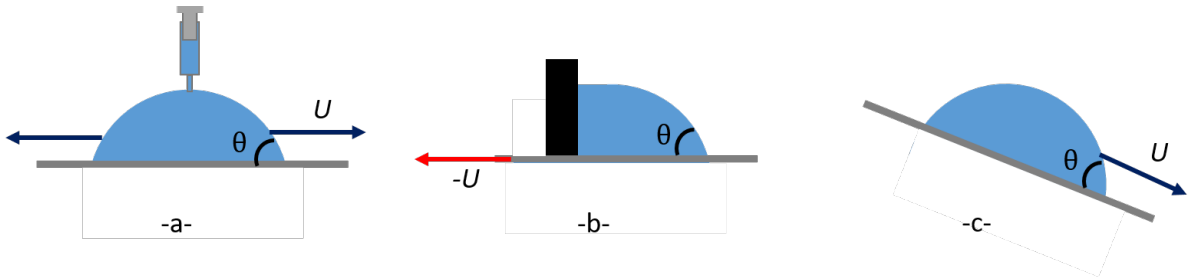

Figure 3: Experimental situations used to measure the dependence of the dynamic contat angle on contact line velocity: (a) the droplet is inflated or deflated, (b) the substrate is moved at velocity U while the droplet is maintained immobile, (c) the substrate is tilted and the droplet is set into motion by gravity. For the sake of simplicity, we assume that the front and rear angles are identical, *i.e.* no contact angle hysteresis.

of the length ratio $\frac{x}{\ell}$ is 10^4. In the experiments with zero equilibrium angles corresponding to the data of figure 4, a precursor film forms ahead of the line; the thickness of the film is then the natural cut-off length ℓ. Its value ranges from 1 to 100 nm, which is consistent with both measurements conducted at a distance x from the contact line ranging from 100 µm to 1 mm and a lengths ratio x/ℓ of 10^4. More details about the microscopic structure of the flow near the contact line can be found in the review by Bonn et al. [6].

In what follows, we focus on effects that modify either the dominant dissipation process or the driving force. The characteristic length scale introduced by those effects may be of the same order as the microscopic cut-off length, as when line friction is at stake, or much larger than the cut off length, when either dissipation in the substrate, Marangoni effects or finite-size effects dominate the dynamics.

3 Line friction and retardation mechanisms

An alternate dissipative mechanism to viscous friction may arise from thermally activated displacements of the contact line, either at a molecular [17] or a mesoscopic scale. [18] The primary motivation for the development of the molecular scale theoretical framework, known as molecular kinetics theory, was to solve the apparent contradiction between a zero-velocity

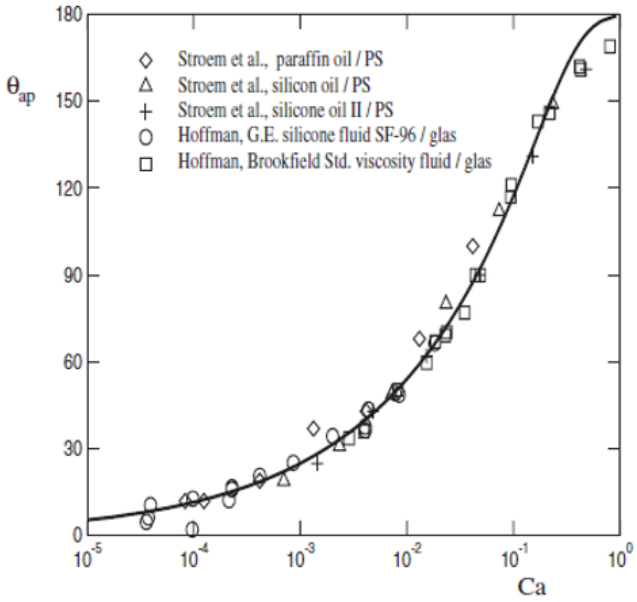

Figure 4: Contact angle as a function of the capillary numbers for different experiments in total wetting conditions. The full line represents equation 6 with $\frac{x}{\ell} = 10^4$. Reproduced from Bonn *et al.*[6]

boundary condition at the solid interface and a moving contact line. At the solid interface, as depicted in Fig.5, molecular adsorption of the advancing liquid and molecular desorption of the receding phase are described within an Eyring framework : molecular jumps between sites are thermally activated and the energy landscape between adsorption states exhibits activation barriers E^* that are biased by the driving capillary force $\gamma(\cos\theta_e - \cos\theta_m)$ where θ_m is the microscopic contact angle. The process is characterized by the mean distance λ between adsorption sites that is expected to be smaller than 1 nm. The jump frequency K^0 is set by the biased activation energy. This molecular mechanism should therefore depend on surface chemistry, *i.e.* molecules adsorbed at the solid surface, or in other words, on the preparation of the surfaces.

An alternate description was offered where the elementary displacements of the contact line occur at mesososcopic scale[19] and are set by the depinning of the contact line from defects or heterogeneities of the solid surface. This picture reconciliates the description of contact line dynamics with the existence of a static contact angle hysteresis[18] in the particular case of non-viscous liquids. In this framework λ is a correlation length of the disorder,

and, as such, may be larger than the nanometer size, and E^* is the energy barrier between two pinned configurations of the triple line on defects. As for the molecular mechanism, the energy barrier sets the attempt frequency of the jumps K^0.

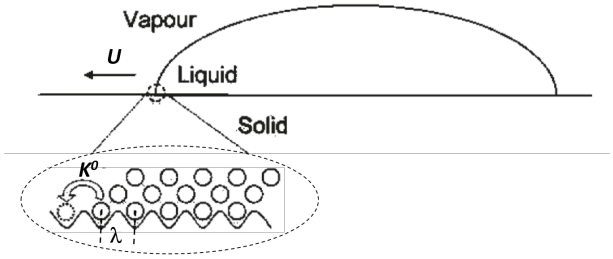

Figure 5: Liquid droplet spreading : Molecular kinetics model. Schematic representations of molecular jumps between sites distant by λ with attempt frequency K^0. Adapted from Goossens et al. [20].

As carefully summarized in the review by Bonn *et al.*,[6] the rate of dissipation by the processes acting at the contact line sets the microscopic contact angle θ_m in the immediate vicinity of the line. This rate is often recast into a friction term, ζU, where ζ is a friction coefficient in Pa.s, so that :

$$\gamma \left(\cos\theta_e - \cos\theta_m\right) = \zeta U \tag{9}$$

In this view, the friction coefficient accounts for all localized dissipative mechanisms. In the activated kinetics view, ζ is related to the elementary jumps length λ and frequency K^0 through $\zeta = \frac{kT}{\lambda^3 K^0}$. A combination of hydrodynamic and molecular effects has been proposed,[21] where viscous dissipation sets the relationship between the macroscopic angle θ and the capillary number through Eq. 6 but in which friction at the line simply appears as a correction to the microscopic contact angle measured at vanishing speed and is set by Eq. 9. For liquids spreading in air, we obtain:

$$\theta^3 - \left[\arccos\left(\cos\theta_e + \frac{\zeta U}{\gamma}\right)\right]^3 = 9Ca\ln\frac{x}{\lambda} \tag{10}$$

This combined model can be conveniently extended to liquid/liquid/solid systems using Eq. 7 instead of Eq. 6. Alternate combined models have been proposed where dissipative mechanisms are additive.[22]

Very recently, rather than analytical expressions, Blake et al.[23] derived an iterative procedure to treat the angle-velocity data with a model combining the two dissipative mechanisms.[23]

Stepping out of the combined model, it is worth emphasizing that the limits within which activated dynamics model and the hydrodynamics model - referred to as Cox-Voinov in the present review - apply are still debated. A transition between hydrodynamic dissipation and contact line friction is predicted by some theoretical works[24] as the contact angle decreases during spreading, but this view is sometimes experimentally validated[11,25–27] or challenged.[28,29] When observed, the transition is measured to be set by a critical capillary number, as experimentally measured[11,25–27] although no consensus exist on its value. It is very likely that the crossover will depend on the ratio between the friction coefficient ζ and the viscosity, as pointed out by De Ruijter,[22] rather than by a definite value of the capillary number that would be valid for all systems.

Other experiments evidenced friction at the contact line, as defined by Eq. 9, but it was not always ascribed to a thermally activated process: some studies relate instead the phenomenological friction coefficient ζ to large-scale (micrometer) surface heterogeneities at the solid surface.[29,30] In experimental systems where great care was taken to gain control on the state of the solid surface (chemical homogeneity and impurities; partial, pseudo-partial or total wetting regime) with well-designed topological defects (spherical caps with typical width 100 nm and height ranging from 10 to 100 nm), and controlled contact angle hysteresis using polymer brushes adsorbed at the solid interface, the authors conclude that there is no evidence of thermal activation specifically due to added defects.[31] Instead, Lhermerout and Davitt[31] offer that energy dissipation takes place in the swollen polymer brush, a mechanism that will be further discussed in Section 4, and that would introduce another length scale

setting the activation length. Finally, the authors point to the need of new experimental methods allowing to discriminate between chemical and topographical heterogeneities, or address collective effects in contact line pinning.[32]

Whether it involves contact-line friction or hydrodynamic dissipation, contact line dynamics appears to involve a micro- or mesoscopic scale that either sets the activation length or the flow boundary condition. In this view, it is crucial to gain a good control on the physico-chemistry of each of the three phases : molecular or topographical heterogeneities of the substrate, slip length or molecular ordering at solid interfaces, prewetting films ahead of the line, evaporation, condensation or surface/bulk diffusion of the liquid(s). Below, the relevance of the precise control of the physico-chemistry of the experimental systems in terms of activated dynamics will be further discussed along three lines : prewetting films, heterogeneities and transfers of surface-adsorbed molecules, and, finally, electrostatic surface charges.

3.1 Molecular adsorption mechanisms and prewetting films

To the best of our knowledge, the possible presence of precursor films is rarely acknowledged in studies reporting measurements of friction at the contact line.[27] Few studies couple the characterization of wetting dynamics to observations of the structure of the liquid close to the contact line at the nanometer scale.[35] However systems such as high energy surfaces (clean glass, silica or native oxide layer of silicon wafers in air...) are likely to exhibit total wetting conditions and to give way to the existence of a prewetting precursor film. In such a case, molecular or depinning jumps are expected to be drastically modified. An example is shown in Fig. 6. For droplets consisting of polarisable polymer melts spreading on silicon wafers, observations of the wetting dynamics at the macroscopic scale proves the existence of an equilibrium contact angle[33] while measurements at the microscale reveals the presence of a nanometer-thick precursor film.[34,36] This system is a case of the so-called pseudo-partial

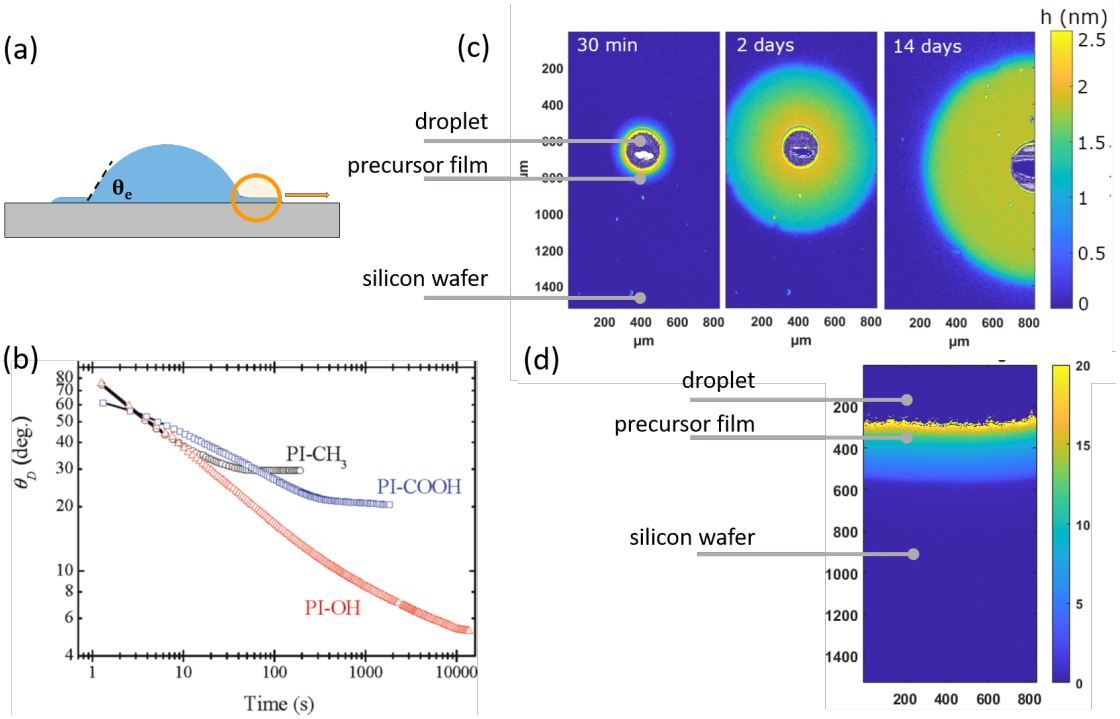

Figure 6: (a) Pseudo-partial wetting of polyisoprene (PI) melts on oxidized silicon wafers with varied terminal end-groups. (b) Dynamic contact angle decreases over time towards a finite non zero contact angle. Data can be fitted to a friction model as in Eq. 9. From Liu et al.[33]. Depending on the end groups, both equilibrium contact angle and friction ζ vary. (c,d) Ellipsometric microscopy images from Schune *et al.* showing a prewetting precursor film of nanometer thickness h spreading (c) around a small droplet of PI-OH over time[34] and (d) a the edge of a large droplet of PI-CH3. The equilibrium contact angle, the dynamics and the precursor film thickness (or molecular surface density) all strongly depend on the terminal groups. Note the thickness scale change between (c) and (d).

wetting state[37,38] that can be detected only if observations at the nanoscale are performed. The analysis of both the dynamics and the statics should integrate this peculiar boundary condition.

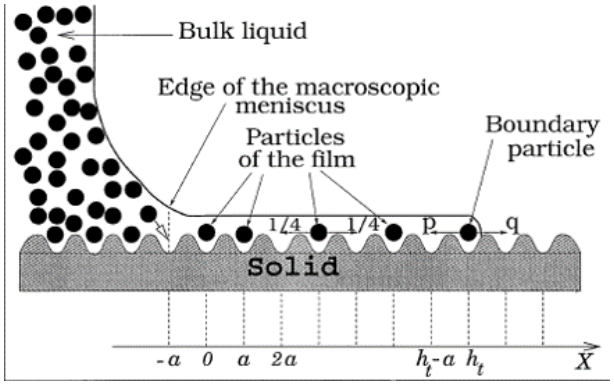

Figure 7: Precursor films : Schematic representations of molecular jumps between sites distant by a with probabilities p, q to model the thermally-activated spreading of molecular thin films on a solid wall connected to a reservoir. Reproduced from Burlatsky et al.[39].

Similar molecular dynamics arguments as those invoked in molecular kinetics theory, depicted in Fig.5, appear in the modelling of both wetting dynamics and precursor films spreading,[39,40] as depicted in Fig. 7. Measurements of the activation energies of molecular jumps at the solid surface, obtained from the spreading dynamics of the molecularly-thin films that consisted of quasi-2D gases, validate the latter description.[36] These observations demonstrate that thermally activated motion of molecules at the contact line are very effective at pulling a film of molecular thickness out of the drop (Fig. 7) rather than setting the whole liquid corner in motion. We note that experimental works have shown that prewetting films evolves from 2D-gases at early stages[36] to dense thicker films at later stages.[34] This certainly has consequences on a molecular kinetics interpretation of the spontaneous spreading of droplets : in the former case, free adsorption sites are available while they are not in the latter, meaning that both the length λ and the frequency K^0 of the jumps could be time-dependent. The transition from dilute to dense prewetting films also has consequences for the viscous hydrodynamics model, although to a lesser extent : the cutoff length ℓ in Eq. 6 can be taken as the film thickness and thus increases over time from 1 nm up to 10 nm.

However, the dependence of the $\theta_d(V)$ law on this cutoff length is logarithmic, and hence rather weak. Finally, whatever the dissipative mechanism, the *equilibrium* contact angle is expected to depend also on the solid/air interfacial tension γ_{sv} which of course depends on the coverage of the solid by the precursor film, as theoretically described by Brochard-Wyart et al.[37]. A possible consequence of prewetting films is the striking behaviour of polymer melts known as autophobic wetting:[41,42] it is observed that the contact line recedes after the initial spreading stage of a melt droplet. This effect may result from the time-dependent adsorption of polymers on the solid within the prewetting film.

Altogether, these remarks call for new experimental data combining observations at all scales of the contact line dynamics on well-controlled systems, which are made easier by the recent development of experimental techniques.[31,36,43]

3.2 Desorption of physisorbed molecules from the solid by moving contact lines

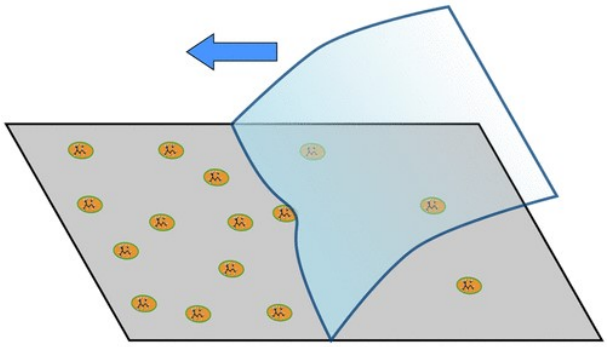

Figure 8: Schematic illustration of a contact line advancing on a solid on which adsorbed molecules form heterogenous patches. (i) If adsorption energies are weak enough, the line desorbs some of the molecules. (ii) The chemical heterogeneities pin the line. Reproduced from Franiatte et al.[44]

As pointed out earlier, we expect molecular dynamics at the contact line to depend not only on the nature of molecules adsorbed at the solid interface, but also on the length scales characterizing their adsorption as well as the anchoring energy of the line on defects. In the

following, we review experimental examples where an additional effect comes into play: the removal of weakly adsorbed species by the contact line itself (Fig. 8). Indeed, the capillary energy associated with a contact line is typically of the order of a few kT so that any molecule or particle desorption process involving activation energies smaller than capillary energies of a few kT is likely to occur. For example, it was recently evidenced that a capillary force at a moving contact line can displace particles,[45] and, in the present review, extraction of mobile free chains from elastomers by contact lines will be reported in Section 4. The two examples we review below demonstrate that the knowledge of the solid surface state at a molecular level is necessary to compare wetting dynamics data with models, but is not sufficient if the moving contact line modifies the surface.

A recent experimental study of the wetting dynamics of oil droplets immersed in water and spreading on silica[46] evidences that cationic surfactants adsorbing to silica considerably slow down spreading. To do so, an oil droplet is pressed onto a silica surface at equilibrium with a surounding solution containaing CTAB at varied concentration. By imaging the wetting of oil using a combination of interferometric microscopy and macro imaging, Rondepierre et al.[46] probed the wetting dynamics over large range of contact angles and velocities (Fig. 9a). They showed that both the static and dynamic wetting data depend on the surface concentration of surfactants at the water/silica interface Γ rather than their bulk concentration. By gently measuring molecular adsorption morphologies (Fig. 9b) with Atomic Force Microscopy (PFT-AFM) Kekicheff and Contal[47] show that surfactant patches with increasing characteristic length grow at the surface of the solid as their bulk concentration increases up to a threshold Γ^*. In this lower range of concentration, the spreading velocity of oil was measured to decrease by several orders of magnitude with increasing surfactant concentration, as reported in Fig. 9a); meanwhile, the statics contact angle showed that the solid was more and more hydrophobic. This apparent contradiction is overcome by showing that the dissipation mechanism at play is a friction localized at the contact line: an

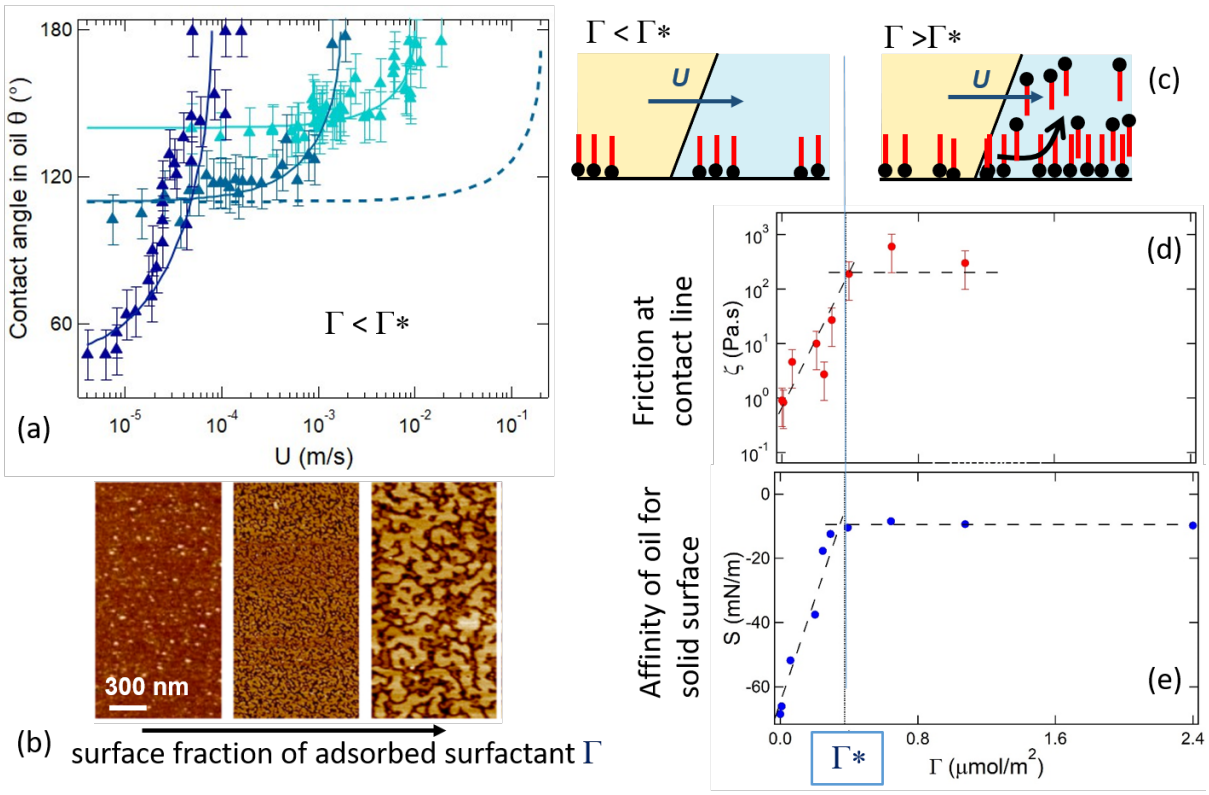

Figure 9: (a) Wetting dynamics of oil on silica in water with CTAB cationic surfactants at concentrations 0, 0.15 and 0.7 times critical micellar concentration from cyan to dark blue.[46] Contact angle versus velocity curves are fitted to the friction model Eq. 9 (lines) with ζ and θ_e as fitting parameters (see d,e). The Cox-Voinov model Eq. 7 (dotted line) fails to fit the data. (b) Morphology of CTAB-laden mica surfaces carefully imaged in water by PFT-AFM by Kekicheff and Contal[47]. As bulk concentration in CTAB increases, surface concentration Γ increases. First, patches of electrostatically adsorbed surfactants grow until Γ^* where a bilayer starts to form through weaker hydrophobic or entropic interactions. (c) Γ^* also separates two wetting regimes : at low Γ, patches of adsorbed surfactants are not modified by the moving contact line, and increase both dissipation ζ and hydrophoby S; at larger Γ, surfactants from the top of the bilayer are desorbed by the moving contact line and no longer contribute to friction or hydrophoby. (d) Contact line friction ζ as a function of surface density of surfactants and (e) Affinity of oil for surfactant-laden silica measured as $S = \gamma(\cos\theta_e - 1)$.[46]

equation similar to Eq. 9 adapted for two fluids, was found to best fit the velocity-contact angle data introducing a line friction coefficient ζ. The friction coefficient ζ increases with the surface concentration of surfactant Γ at the solid/water interface (Fig. 9d) below Γ^* as a consequence of the increased heterogeneity of the silica surface induced by the presence of the hydrophobic surfactant patches. In this low-concentration regime, surfactant adsorption is strong enough that imaging the surface at rest provides a good enough picture of the physico-chemistry of the interface at molecular scales to draw a link with friction and hydrophoby. Indeed, at low concentration, adsorption involves electrostatic interactions that are usually stronger than capillary energies, of order 1 to 10 kT. Hence, adsorbed surfactants are unlikely to desorb under the action of the moving contact line.

However, weakly adsorbed surfactants may desorb, and this is what is observed above the threshold concentration Γ^*, where the first monolayer is now complete. Above Γ^* additional surfactants start to form a double layer and adsorption then proceeds through weak entropic (or hydrophobic) interactions. Conversely, both the spreading parameter $S = \gamma\,(\cos\theta_e - 1)$ of oil and friction coefficient ζ no longer depend on the surfactant concentration. They stick to the value set by the first strongly adsorbed monolayer underneath. Hence the oil/water/solid contact line is found here to be able to desorb weakly adsorbed molecules.

The desorption of molecules from a solid surface by moving contact lines is also evidenced in an air/liquid/solid configuration where the solid exposed to the atmosphere is contaminated by traces. To do so, Franiatte et al.[43],[44] use AFM tips shaped as needles of radius $60 < r < 300$ nm that are dipped into and retrieved from a droplet at constant velocity U. By measuring the force exerted on the tip by the contact line, the authors first demonstrate that contact line motion displays discontinuities that reveal topographical defects on the tip surface. These topographical defects are characterized by a nanometer-sized lengthscale that is used in the modelling of the dynamics of the whole contact line: the velocity dependence of the capillary force obeys an activated dynamics model as in Eq. 9. One major contribution

of this work is the discrimination between the effects of topography and the chemistry of the defects. Indeed, the authors show that the nature and number density of molecules physically adsorbed on the silicon oxide layer of the AFM tip set the amplitude of the activation barrier E^* in the kinetics model while topography sets the lengthscale λ. One other major finding is that physisorbed molecules, probably airborne short-chain hydrocarbons always present in atmosphere, are efficiently removed after a few tens of dipping-retrieving cycles. As a consequence, both the statics and the dynamics of the contact line are modified, through θ_e and ζ respectively. This effect introduces another velocity-dependence: indeed, the desorption by the contact line shifts the adsorption equilibrium between contaminants in air and at the solid surface all the more as the line moves faster and faster. Hence, the apparent θ_e and ζ measured in ambient atmosphere could vary with velocity and the number of times the line has swept the surface. The authors conclude that desorption of weakly adsorbed contaminants by contact lines could explain the variability often observed in contact angle measurements, especially with polar liquids and high energy surfaces.

Finally, it is worth underlining here the similarity between the mechanisms involved in the capillary-driven desorption of molecules and the Schallamack model[48] for rubber friction where polymer chains are adsorbed across the solid interface, then stretched upon sliding and dissipate energy as they detach. In both cases, the elastic energy stored in the deformation of the contact line in contact line friction and in the stretched polymer chains in elastomer friction is spent in a molecular desorption event : desorption of contaminants in the former case, and of the polymer chain across the moving interface in the latter case. The elastic energy associated with both processes can be estimated[49,50] and is found to be of the order of $10kT$ for most liquids and rubbers, which is enough to break physical bonds but not chemical or covalent ones (of the order of 100 kT).

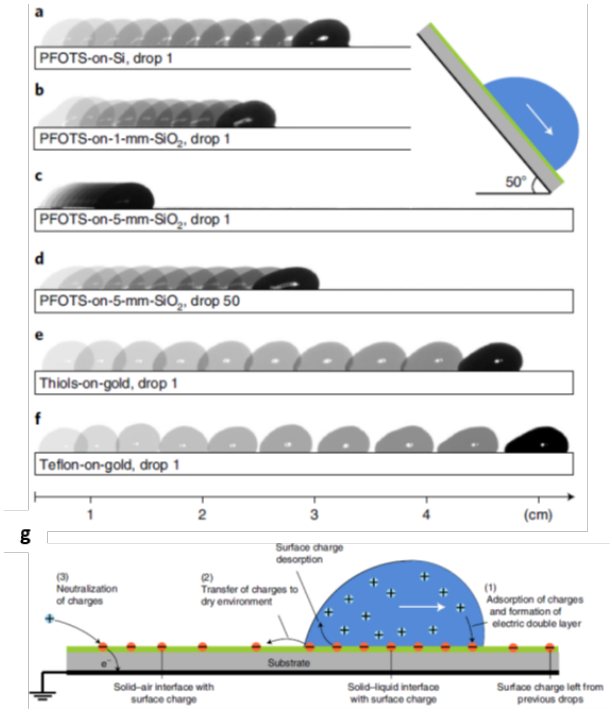

Figure 10: Electrostatic retardation of water drops (33 μm) sliding down a series inclined plates (50°) of varied material and surface treatment. The drop is initially grounded. Images are taken every 10 ms from the side. While silicon (Si) or gold wafers show no electrostatic charge of the drop, silica (SiO_2) plates of low permittivity charge the drop and slow it down. Both the charge and the friction force depend on the slide distance, the substrate thickness, and on the drop number. (g) Schematics of mechanisms involved in the charge transfers and model developped to relate the electrostatic friction force to the interfacial charges deposited at the air-solid interface and to the drop charge. Reproduced from Li et al.[51].

3.3 Electrostatic retardation

Very recently, the motion of sliding droplets of water or other polar liquids on low-permittivity substrates was measured to be substantially influenced by electrostatic forces[51,52] which amount to an extra friction term that can make up to half of the total dissipation measured. The mechanism underlying this electrostatic retardation is ascribed to the deposition of electric surface charges of the substrate behind the sliding drops. For water on hydrophobic surfaces, the drops usually acquire a positive charge while interfacial charges are negative, their origin still being debated. By setting up carefully designed experiments where droplets slide down an inclined plate (Fig. 10a), Li et al.[51] are able to measure the electrostatic retardation force by comparing high and low-permittivity substrates having the same surface treatment. The droplet charges are also measured. These inputs feed a model accounting for the Coulomb force exerted on the charged droplet by the electric field created by the surface charges on top of the dielectric substrate; this model successfully describes droplet motion and the electrostatic friction force[52] (Fig 10g). We believe that these findings shed new light on existing experimental data: indeed, the friction force exhibits several features that have been overlooked so far, such as its dependence on history through the charges left from previous drops (Fig. 10c,d), its non-monotonic dependence on slide length and on the thickness and the permittivity of the underlying substrate (Fig. 10b,c). Furthermore, the experimental systems used by Li et al.[51] are ubiquitous (among others, water, NaCl+water, ethylene glycol as liquids; fluoro-silanated glass or silicon wafer for solids) and found in numerous wetting dynamics studies.[28] We also note that the neutralization of charges at the solid air interface is expected to depend on the ambient humidity, which should then be controlled in dynamic wetting experiments. Finally, Stetten et al.[52] suggest that electrostatic effects on wetting dynamics could extend to hydrophilic and conducting surfaces as well: shorter relaxation times for charge neutralization are expected in these cases and the effect may have remained unnoticed. Yet, even short-term charging may influence wetting dynamics. Experimental data collected on conductive and high permittivity substrates showed however that electro-

statics is negligible:[51] the difference between gold and silicon seen in Fig. 10a,e,f) reduces to a static contact angle effect. The good news is then that past experiments performed on silicon wafers that are semi-conductors were probably not affected by electrostatics.
We believe these findings on electrostatic retardation of wetting dynamics open a wide field for experimental research. The coupling between charge transfers and contact line movement evidenced above could introduce a new length scale setting the activation length. Hence, assessing the charge transport at the solid surface as depicted in Fig.10g-2) could allow for a quantitative modelling of the charge distribution over time and deepen our understanding of the couplings between slide electrification and retardation.

In summary, we have reviewed experiments in which the dynamics of the contact line is coupled with transfers at the molecular scale. The couplings are mediated by chemical adsorption on the solid that results in energy dissipations that are much larger than that by viscous friction, inducing large decreases of the contact line velocity. In the following section, we will also explore alterations to the substrate caused by the moving contact line, but these modifications are of a mechanical nature rather than chemical.

4 Dissipation in the substrate

4.1 Soft non-soluble substrates: deformation at the contact line

We now examine the case in which energy dissipation takes place in the substrate rather than in the liquid, as in Cox-Voinov model (Section 2), or at the contact line, as in Section 3. The Young-Dupré law, given by Eq. 1, accounts only for force components tangential to the solid surface, the normal force balance being left aside. However, very early, Lester[53] shows that the normal component of the resulting capillary forces at the contact line deforms the

solid with a typical amplitude given by

$$h \propto \frac{\gamma}{\mu_0}, \tag{11}$$

with γ the surface tension of the liquid/gas interface and μ_0 the shear modulus of the solid. For solids such as glass, with shear moduli greater than 1 GPa, this deformation is subatomic, and thus negligible. If the shear modulus is rather that of a very soft solid, $\mu_0 \simeq 10$ kPa, and the typical value of the surface tension of the liquid, $\gamma \simeq 40$ mN m^{-1}, we obtain $h \sim 4$ µm.

The resulting ridge formed at the contact line has important consequences on the dynamics of wetting. For example, droplets moving on soft layers covering the surface of a rigid solid slow down compared to the case of the bare surface.[54–57] Since contact line motion imposes that the ridge propagates along the surface of the viscoelastic substrate, energy dissipation in both the liquid and the solid occurs. As a consequence, the velocity of the contact line for a given difference between the dynamic contact angle θ and its equilibrium value θ_e is smaller on a viscoelastic substrate that acts like a viscoelastic brake.[57]

In most experiments, the substrates are made of cross-linked silicone rubbers. Their shear modulus can easily be tuned by changing the cross-linker concentration. They are often referred to as silicone gels, although they do not contain any solvent. We will see later that they contain free (uncross-linked) and tethered chains but in a first approach we neglect the effect of these chains. The rheology of rubbers is characterized by a single relaxation timescale τ. Dimensional analysis of the problem shows that the dynamics of moving contact lines depends on the relative magnitude of energy dissipation in the liquid and the solid[58,59] estimated with the relaxation ratio,

$$\mathcal{R} = \frac{\gamma\tau}{\eta\ell_s}, \tag{12}$$

where η is the viscosity of the liquid and ℓ_s is the elastocapillary length of the solid,

$$\ell_s = \frac{\gamma_s}{2\mu_0}, \tag{13}$$

with γ_s the surface tension of the gel taken as the average between its interfacial tension with the liquid γ_{sl} and its surface tension with the atmosphere γ_{sv}. This length scale is the characteristic amplitude of deformations, since Eq. 11 can be rewritten as $h \propto (\gamma_{lv}/\gamma_s)\ell_s$. The relaxation ratio is the proportionality factor between the liquid capillary number, Ca, and its solid counterpart, $Ca_s = \mathcal{R}Ca = U\tau/\ell_s$.

To the best of our knowledge, most studies in the literature are performed in the regime corresponding to $\mathcal{R} >> 1$, *i.e.* when dissipation mainly occurs in the solid substrate, and the viscosity of the liquid does not affect droplet motion.[58] Careful measurements of the dependence of the dynamic contact angle θ on the velocity U of the contact line show that they still relate to each other through a power law at small values of the capillary number, with an exponent that differs from that expected in the Cox-Voinov law. Scaling arguments similar to those leading to the Cox-Voinov relation can be used to explain this relation. The capillary power per unit length of the contact line injected in the system is

$$\mathcal{P}_{in} \sim \gamma U(\cos\theta_e - \cos\theta). \tag{14}$$

The ridge has a typical cross-section ℓ_s^2. At frequency ω, the dissipated power per unit length in the ridge scales as

$$\mathcal{P}_d \sim \mu'' \omega \epsilon^2 \ell_s^2, \tag{15}$$

where ϵ is the scale for strain and μ'' the loss modulus of the substrates. The loss modulus of the silicone gels used in experiments is a power law of frequency, $\mu'' = \mu_0(\omega\tau)^m$. Taking $\epsilon = \gamma/\gamma_s \sin\theta$ as a scale for strain and $\omega = U/\ell_s$ as the typical frequency at which the contact

line deforms the solid, we obtain

$$\mathcal{P}_d \sim \mu_0 \left(\frac{U\tau}{\ell_s}\right)^m U\ell_s(\frac{\gamma}{\gamma_s}\sin\theta)^2. \tag{16}$$

Equating Eq. 14 and 16, the following relation is finally found

$$f(\theta) \propto \frac{\gamma}{\gamma_s^2}\mu_0\ell_s(\mathcal{R}Ca)^m, \tag{17}$$

with

$$f(\theta) = \frac{|\cos\theta - \cos\theta_{eq}|}{\sin^2\theta_d}. \tag{18}$$

The absolute value allows comparison of data obtained for advancing and receding contact lines.

Figure 11 shows that this scaling law is in good agreement with available experimental data[60–63] for the dynamic contact angle θ at small contact line velocities over silicone substrates with different properties. Note that this figure shows data for which we were able to retrieve all the parameters to compute $\mathcal{R}$. Other data follow the general dimensionalized law $f(\theta) \propto Ca^m$.[64]

The experimental data deviate from Eq. 17 at the largest values of the solid capillary number. The slope decreases as Ca_s increases. In this regime, the characteristic timescale of the flow is smaller than the relaxation timescale of the substrate. As a consequence, the storage and loss modulii of the gel are of the same order of magnitude and both contribute to its apparent stiffness that increases with frequency. The size of the ridge is constrained, and so is dissipation. Recent insights obtained from a non-linear description of the problem[59] suggest that the curve tends toward an asymptotic value,

$$f(\theta) \xrightarrow[Ca_s\to\infty]{} \frac{\gamma}{\gamma_s}\frac{m}{1-m}. \tag{19}$$

This equation still requires extensive testing as only a limited set of data for the saturation

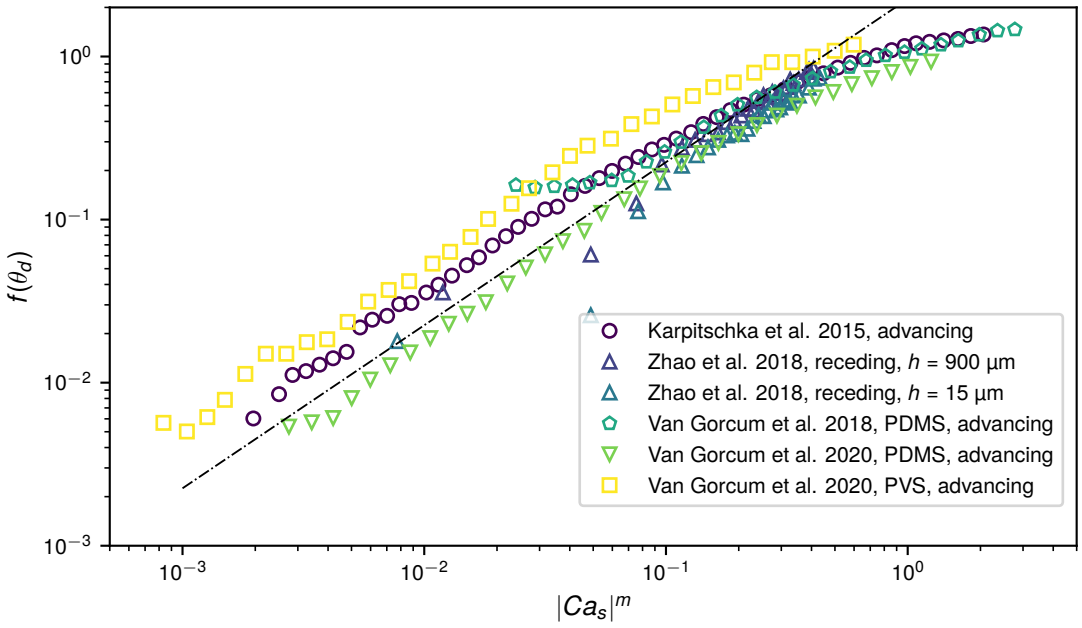

Figure 11: Summary of available contact angle data sets plotted as a function of the m-th power of the solid capillary number Ca_s, where m is the exponent appearing in the loss modulus of the substrate. Properties of the substrate: ○ shear modulus $\mu_0 = 1200$ Pa, relaxation time $\tau = 130$ ms, loss exponent $m = 0.55$;[60] △ $\mu_0 = 1.08$ kPa, $\tau = 15.4$ ms and $m = 0.626$;[61] ⬠ $\mu_0 = 265$ Pa, $\tau = 480$ ms and $m = 0.61$;[62] ▽ $\mu_0 = 390$ Pa, $\tau = 540$ ms and $m = 0.58$ and □ $\mu_0 = 415$ Pa, $\tau = 80$ ms and $m = 0.61$.[63] We were unable to find the value of the equilibrium contact angle of the liquid on the PVS sample. As this material is similar to PDMS, we assume that $\theta_{eq} = 105$ °. Dot-dashed line: scaling given by Eq. 17.

exists. Finally, the contact line enters a stick-slip regime[60,62,65] in which it detaches from the tip of the ridge and moves fast until another ridge has had the time to grow.

Energy dissipation in the substrate may be an advantage or a drawback in applications. Several system parameters provide control over dissipation. For example, when the substrate is a layer of rubber coating a rigid substrate, Zhao et al.[61] report a decrease of dissipation as the thickness h_0 of the rubber layer decreases. They interpret this observation as a finite-depth effect that results in the decrease of the ridge height as the the layer is thinner. This effect becomes prominent when $h_0 \leq \ell_s$. They suggest that, in the latter regime, the relevant length scale for the height of the ridge is

$$h = \left(\frac{\gamma_s h_0^3}{\mu_0}\right)^{1/4} \tag{20}$$

rather than ℓ_s. A scaling model describing the motion of the contact line for thicknesses of the order of the elastocapillary length well captures the decrease of dissipation. More recent work by Khattak et al.[66] shows that scaling 20 fails when $h_0 << \ell_s$. Indeed, the strain h/h_0 diverges as the thickness decreases, and the deformation cannot be described in the frame of linear viscoelasticity. Khattak et al.[66] suggest a scaling based on the assumption that the height of the ridge is proportional to h_0, which seems to capture the trend of the experimental data. Another way to tune the amplitude of the ridge is to stretch the soft layer. Snoeijer et al.[67] measure the dynamic contact angle and show that the contact line moves faster on the stretched substrate than on that undeformed for a constant value of the dynamic contact angle. Smith-Mannschott et al.[68] show that droplets slide the fastest down a vertical stretched sheet when the stretch direction is parallel to that of gravity. They measure the surface profile of their stretched layer around the droplet (Fig. 12a). They observe that the amplitude of the ridge is the smallest along a line passing through the centre of the droplet and parallel to the stretch direction. Here too, a smaller ridge results in a smaller dissipated energy.

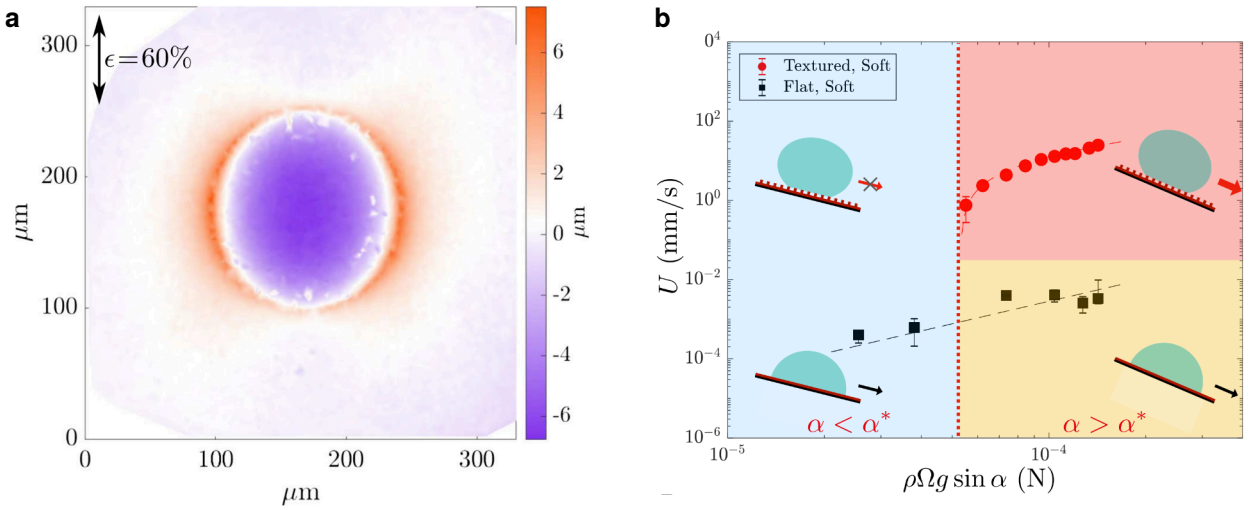

Figure 12: (a) Profilometry of the surface of a stretched soft layer around a sessile droplet. Applied strain $\epsilon = 60\%$. Taken from Smith-Mannschott et al.[68]. (b) Velocity of a droplet sliding on a textured soft surface and on a smooth soft surface as a function of the inclination of the surface. Reproduced from Coux and Kolinski[69].

Another path to control dissipation is to texturize the surface of the substrate. Coux and Kolinski[69] show that the motion of droplets sliding down the surface of a soft silicone gel patterned with pillars is insensitive to viscoelastic braking. They demonstrate that the solid contribution to dissipation is small because the droplet contact line induces significant deformations of the solid only at its trailing-edge contact line, *via* pillar bending. The associated dissipation is orders of magnitude smaller than that in the liquid. Hence, only the latter contributes to the dynamics of the droplet, and droplets slide on patterned soft surfaces orders of magnitude faster than on smooth ones (Fig. 12b).

The description of the dynamics of wetting on soft viscoelastic solids yielding Eq. 17 date back to the 1990's[56] and rely on a linear viscoelastic description of the substrate: the deformations of the gel are assumed infinitesimal. Within this framework, surface slopes on the gel are proportional to the ratio of the surface tensions of the solid and the liquid, γ_s/γ. Hence, the validity of a linear viscoelastic description is only guaranteed when:

$$\frac{\gamma_s}{\gamma} << 1. \tag{21}$$

This condition is never met in experiments, since the surface energy of the materials commonly used is of the same order of magnitude as or larger than that of the liquid. Although a model based on linear viscoelasticity can capture the general trends observed in experimental data, it falls short when it comes to providing a quantitative description.

Non-linear descriptions accounting for the finite value of γ_s/γ have been proposed in recent years, based on different hypotheses regarding the conditions at the surface of the solid. One of these models,[70] which assumes that a stress singularity exists at the tip of the ridge, is able to describe quantitatively the statics of wetting on soft solids without any adjustable parameter. Similar models for the dynamic case have been proposed.[59,71] The predictions of Dervaux et al.[59] have been tested against experiments with success,[72] in particular by exploring the relation between the relaxation ratio $\mathcal{R}$ and the properties of the moving contact line. However, these problems have to be further explored, in particular in light of the properties of the rubbers that are used in wetting experiments. As pointed out above, they generally contain free polymer chains and we emphasise in the following section the consequences of the presence of this liquid, which results in transfers of molecules from the soft solid to the liquid/air interface.

4.2 Coupling of dissipation in the substrate with molecular transfers

4.2.1 Capillary extraction of free chains from rubbers

The silicone rubbers or "gels" used in all of the wetting experiments we have reviewed so far are easy to prepare, rather insensitive to surface contamination by impurities and their mechanical properties are easy to vary and control. However, their formulation is hardly controlled, in sharp contrast with the care with which elastomers are usually prepared in the adhesion and friction community.[73,74] In wetting experiments, the mechanical properties of the silicone gels are tuned by changing the mass ratio of the curing agent and silicone

oil. This change in the formulation comes at the expense of an increased amount of mobile chains in the sample. For example, Sylgard™ 184 prepared under recommended conditions contains around 5wt% mobile chains.[75] A gel prepared with the same kit with 1 volume of curing agent for 60 volumes of base PDMS contains more than 50wt% mobile chains.[76] Methods to extract mobile chains without damaging soft samples[77] have been developed only very recently,[76] hence many wetting experiments of the literature have been conducted in presence of mobile chains.

Recent investigations show that these mobile chains also play a crucial role in the dynamics of wetting on silicone elastomers, as could have been expected from early studies on the adhesion of elastomers: free mobile chains were shown to play a crucial role in their effective interfacial energy.[78,79] Hourlier-Fargette et al.[75],[80] show that droplets residing on a stiff Sylgard™ 184 gel can extract part of the small amount, 5wt%, of mobile chains present in the substrate. The typical extraction timescale induced by a moving droplet is much shorter than when the droplet is sessile. This extraction has a direct consequence on droplet motion. The velocity of a droplet sliding on a vertical non-extracted silicone sample changes over time from a small constant value up to a higher one. Hourlier-Fargette et al.[75] argue that this transition is related to the contamination of the liquid/gas interface of the droplet by mobile chains coming from the substrate. Indeed, a droplet sliding on a "dry" slab of gel from which mobile chains were extracted moves with constant velocity. The authors relate the time at which the transition occurs to the saturation of the liquid/gas interface with mobile silicone chains. As a result, the surface tension γ decreases as well the equilibrium contact angle. Images of the droplet before and after the transition show no significant change of the dynamic contact angle, suggesting that the decrease of the surface tension of the droplet leads to an abrupt increase of the capillary energy injected in the system, hence a sharp increase in the velocity.

Mobile chain extraction has since then received significant attention. Wong et al.[81] bring evidence that their extraction induces a two to threefold increase of the contact hysteresis

of PDMS samples. They highlight the lubricating role of mobile chains. An investigation of the hysteretic response of the extracted samples in connection with the known increase of the roughness of PDMS samples after extraction would be interesting.[82]

Confocal microscopy reveals the extent to which mobile chains contribute directly to the ridge. Dying the cross-linked PDMS network and the silicone oil with two different fluorophores, Cai et al.[83] show that mobile chains occupy an increasing fraction of a static ridge as their amount increases in the substrate. A key finding is that the deformation of the cross-linked network is a non-monotonic function of the swelling amount. Hauer et al.[84] extend these observations to the case of a moving contact line. They show that silicone oil occupies a smaller fraction of the ridge as the contact line moves faster. They attribute this dependence to a competition between diffusion of the mobile chains in the cross-linked network and their advection by the contact line. These results suggest that the lubricating role of the mobile chains identified by Wong et al.[81] may depend on the velocity of the contact line.

These observations imply that the substrate should rather be described within a poroelastic framework in which the liquid inside the gel rearranges when the substrate is under stress. Such a description exists and has been tested to some extent for equilibrium.[85–87] To the best of our knowledge, a similar description for dynamic situations does not exist yet. A poroelastic description will also be interesting for solids containing solvents such as hydrogels.

4.2.2 Soluble substrates

Transfers associated with a higher dissipation in the substrate than in the liquid also take place in soluble substrates. Indeed in this case, in contrast to the preceding section, it is the wetting solvent that is transferred to the substrate. When a drop of solvent spreads over a polymer substrate, both its contact angle and velocity are reported to decrease with time.[88] The angle is plotted as a function of velocity in Figure 13 for water spreading on a micron-

thick polysaccharide layer. The corresponding capillary number remains very low: neither the surface tension nor the viscosity of the water droplet varies significantly over the course of the experiment, so the capillary number is at most 10^{-5}. Consequently, viscous dissipation is found negligible and the Cox-Voinov law fails at explaining the large angle variations with velocity that are reported. In fact, the dynamics is governed by the solvation of the substrate ahead of the contact line, which can be measured from thickness variations as displayed in Fig. 13. When spreading starts, the polymer layer is weakly hydrated and behaves like a rigid hydrophobic substrate. The spreading angle decreases as more water is transferred to the substrate. Towards the end of spreading, the substrate has a high water content and the contact angle tends towards zero. Since the hydration of the substrate depends on the velocity of the drop, the angle also depends on the velocity. More precisely, in this picture, the contact angle coincides with the equilibrium angle $\theta \simeq \theta_e$. The equilibrium angle itself depends on the volume fraction of solvent in the substrate, $\theta_e = \theta_e(\phi)$ since the surface energies of the liquid/substrate and air/substrate interfaces should depend on this. The solvent content varies with drop velocity, $\phi = \phi(U)$ and, finally, the angle varies with velocity, $\theta = \theta(U)$, although viscous dissipation is negligible. Note that the amplitude of angle variations are much larger for polar than nonpolar solvents. In the former case, the polymer layer behaves as a solvophobic substrate at the early stages of spreading since polymer chains at the interface with air tend to exhibit their more nonpolar parts. Hence, changes in the surface tension of the solvated solid were shown to be set by characteristic times that depend on the polymer molar mass : shorter chains reorient their polar groups faster than longer ones.[89] This effect does not exist with nonpolar solvents for which angle variations were found to be smaller.[90]

If the polymer substrate is initially in a glassy state, large variations in solvent content can trigger a glass transition during spreading[91] through a plasticization effect. The substrate becomes highly viscoelastic in the glass transition region and is then significantly deformed by the contact line. Dissipation occurs in the substrate as the contact line moves, the onset of

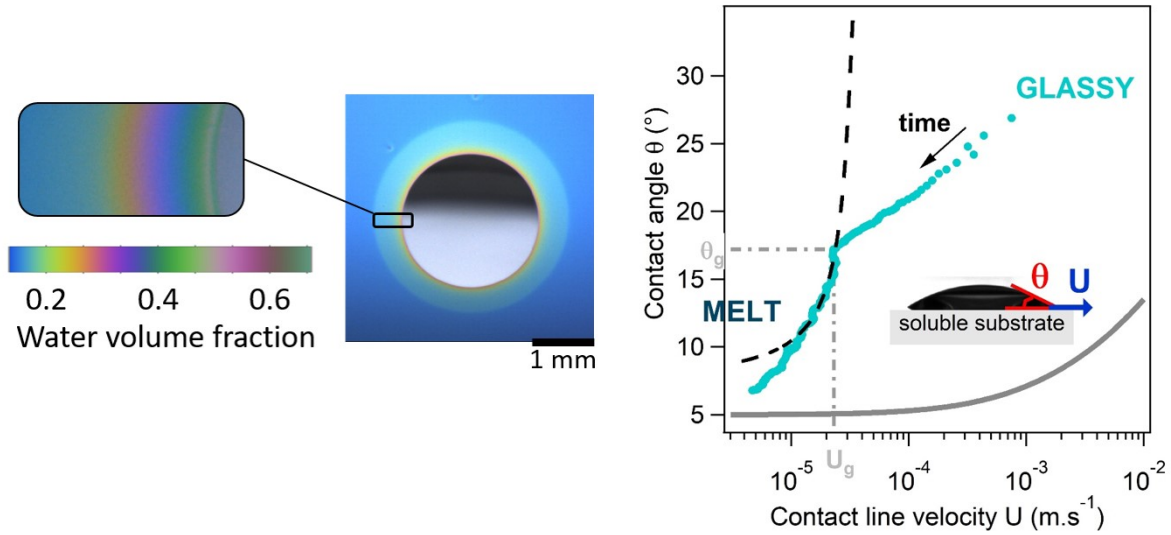

Figure 13: (left) Top view of a droplet spreading on a thin soluble substrate. The colors ahead of the contact line reflect the increased thickness and thus the hydration (color scale) of the substrate. (right) Contact angle as a function of velocity of a drop of water spreading onto a soluble polysaccharide layer. The polymer is initially glassy and glass transition occurs in the course of spreading, when the velocity reaches a value U_g corresponding to an angle θ_g. The dynamics is then partially described following Eq. 17 with $m = 0.75$ (hatched black line). Cox-Voinov law is shown for an equilibrium angle arbitrarily chosen of 5° (grey full line). Adapted from Dupas et al.[91].

which is revealed by a large slope change in the angle vs. velocity curve (Fig.13): the contact angle suddenly drops at decreasing velocities (corresponding to increasing time), because energy is strongly dissipated. Spreading may even stop as the contact line is pinned by the ridge, as observed with drops of toluene spreading on polystyrene.[90] Although a quantitative description is difficult because the driving force and mechanical properties keep varying with time, the variations of the angle can be locally described by accounting for dissipation in the substrate in the same way as for nonsoluble substrates, following Eq. 17. Accordingly, the velocity U_g corresponds to a viscosity of the substrate in the melt phase, just above the glass transition. In summary, the spreading of solvent drops on glassy soluble substrates can be strongly modified by the occurrence of a glass transition in solvent content by turning the substrate into a soft, highly dissipative medium. Away from the glass transition region, the contact line modifies the properties of the substrate as it moves, which in turn rules the wetting dynamics. Wetting of soluble substrates therefore constitutes a case of reactive spreading.[92]

In the Sections 3 and 4 of this review, we have considered effects on wetting dynamics arising - at least partly - from the properties of the wetted substrate, such as roughness, adsorbed species, induced charges or viscoelasticity. In the following two sections, we consider effects that originate from the composition of the liquid.

5 Surfactant-induced Marangoni effect

Marangoni effects are negligible when a drop spreads on a substrate on which surfactants have previously adsorbed, as reviewed in Section 3.2. In contrast, these effects can be at play when a droplet of surfactant solution spreads on an initially bare substrate. Numerous studies have addressed the wetting behavior of surfactant solutions, with considerable attention directed towards surfactants that promote water spreading on low-energy hydrophobic

surfaces such as polymeric surfaces. Water droplets are expected to only partially wet these materials, but, in contrast, droplets of aqueous solutions of specific surfactants completely wet these substrates. These surfactants are called superspreaders, and they have been the object of extensive research.[93,94] In contrast, other surfactant solutions were shown to have wetting behaviours close to the one of pure water,[95] although small differences in the wetting dynamics were observed,[96] which could not simply be accounted for by the modification of the surface tension and equilibrium angle.

Obviously, the presence of surfactants can result in Marangoni stresses at the surface of the spreading drop provided concentration gradients are created. A naive picture suggests that the existence of a region depleted in surfactant close to the contact line would result in a surface stress directed towards the contact line, and consequently in a faster flow than in the pure liquid case. In contrast, the shear induced by the Marangoni stress is predicted to modify the flow in the drop and to lead to a dissipation larger than in the free-surface flow with the same average velocity.[97] Marangoni stresses therefore results in a slower wetting dynamics. To the best of our knowledge, this counter-intuitive result has received little attention while it seems consistent with experimental observations. For instance, Tanner's law for droplets of AOT solutions has a prefactor smaller than that of pure water.[96] The effect remains moderate, in agreement with the weak modification of dissipation that is expected.

To understand the behaviour of superspreaders, adsorption of surfactants at the liquid/solid interface must be accounted for. As the contact line progresses, a flux of surfactants toward the substrate is established that may be sufficient to maintain a surfactant-free region at the contact line. The role of adsorption at the solid surface in superspreading has been emphasised by different authors who developed models,[98–100] but there is still no unanimity in the exact mechanism.[101,102] Plausibly, as pictured in Figure 14, the strong Marangoni stress at the depleted region curves the interface in this region and it is the capillary force on that curved "clean" interface that drives the wetting, augmented by a contribution of the

Marangoni stress.[100] Therefore, the wetting dynamics is Marangoni-enhanced. In addition, this effect can exist only for a range of surface concentration; the "sink" effect produced by the absorption at the substrate needs actually to be larger than surfactant advection toward the contact line; the flux of surfactant from the interface with air to the substrate must therefore be larger than a minimum value.[97,99,100] At the same time, the flux must be smaller than a maximum value in order for the depleted zone to be confined in a small region close to the contact line, yielding a large concentration gradient and an efficient Marangoni flow. For a soluble surfactant, the condition on the flux results in a condition on the depletion length Γ_0/c_0, where Γ_0 and c_0 are respectively the surface and bulk concentrations. The latter condition is consistent with the fact that only few surfactants are superspreaders[100] and that adsorption at the solid surface is not sufficient to induce superspreading. Available models need to be further compared to experimental findings and in particular to measurements of the angle variations with velocity.

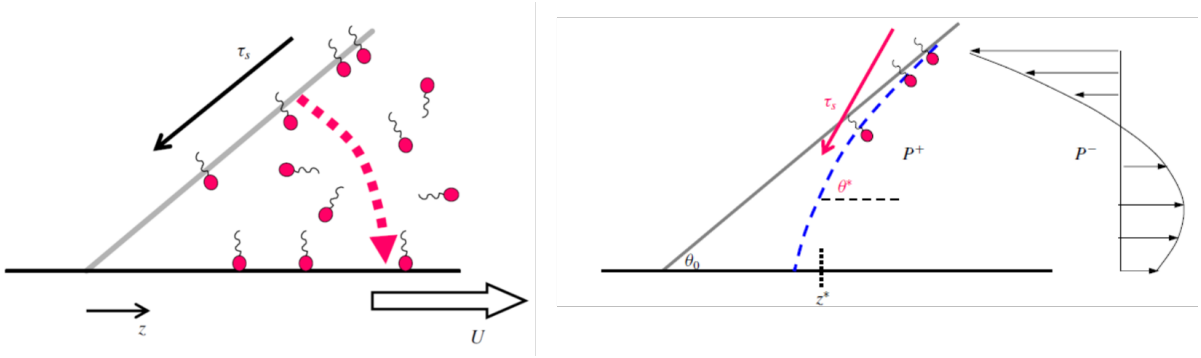

Figure 14: Sketch of the region depleted in surfactant close to the contact line, which is maintained by a flux toward the substrate (left) and on which the resulting Marangoni stress induces a curvature of the contact line (right). Note that adorbed surfactants are schemed as expected for a hydrophilic surface since the described mechanism does not reduce to superspreaders. Reproduced from[100]

In summary, as a drop of surfactant solution spreads, a region depleted in surfactant is created at the contact line. The associated Marangoni shearing modifies the flow in the drop, which tends to increase viscous dissipation and slow down the dynamics (or increase the angle if the velocity is imposed) without significantly altering the shape of the contact line.

In contrast, if the surfactant adsorbs at the solid substrate, the region depleted in surfactant is sustained by the associated "leak" and the large Marangoni stress that results deforms the contact line, which in turn modifies the wetting dynamics and may allow spreading on hydrophobic substrates.

In the next section, we consider liquids containing suspended particles, in which a depleted region also forms close to the contact line. The driving effect is then of steric origin instead of a surface tension gradient.

6 Finite-size effects

Complex fluids such as suspensions of rigid particles, emulsions and foams are characterized by a characteristic mesoscopic length, which is the size of the dispersed objects d. This size can vary from values typical of the colloidal regime, $d << 10^{-6}$ m, up to the millimeter, and can be commensurate with the height of a spreading droplet. It is then natural to wonder how the presence of these objects alter the dynamics of wetting depending on their size. Surprisingly, this question has received little attention. In addition, dispersed systems exhibit complex rheological behaviours and, sometimes, unusual boundary conditions for flows. In this Section, we review examples where finite-size effects in dispersed systems play a role in the wetting dynamics of droplets, either through confinement effects or changes in the flow close to the contact line.

6.1 Confinement due to finite-size effects

In this part, we review the coupling between confinement effects and wetting dynamics. Confinement is here defined by the ratio between the height h of the liquid wedge as depicted in Fig. 2 and the typical size characterizing a dispersed phase. As a first example, we explore density-matched suspensions of non-Brownian particles, starting with viscous granular suspensions in the dense regime where the particle volume fraction is large, typically $\phi \geq 20\%$,

and as well as the particle diameter $d_p \geq 10$ µm.

Zhao et al.[103] study the dependence of the contact angle of a droplet of granular suspensions on the velocity of the contact line. The suspensions they use are Newtonian liquids, with a surface tension identical to that of the suspending liquid.[104,105] Their viscosity η_s is proportional to that of the continuous phase:[106]

$$\eta_s = A\eta_0, \tag{22}$$

with A an empirical prefactor that depends on the particle volume fraction ϕ and its distance to the critical particle volume fraction ϕ_c at which the bulk viscosity of the suspension diverges. In contrast, η_s does not depend on the particle size.[106]

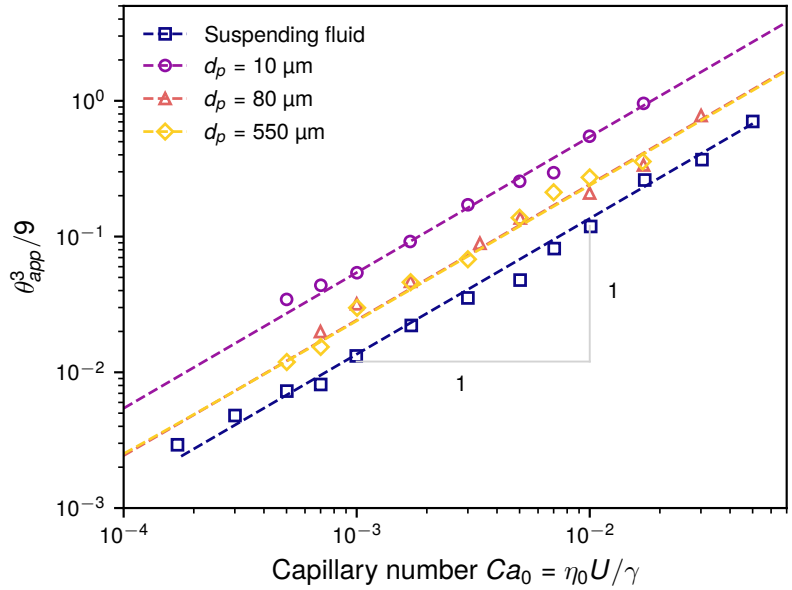

Figure 15: Dynamic contact angle of a droplet of granular suspension spreading on a silicon wafer as a function of the suspending liquid capillary number, $Ca_0 = \eta_0 U/\gamma$. Markers represent data while dashed lines are fits to the Cox-Voinov relation Eq. 6. Data from Zhao et al.[103].

As shown in Fig. 15, the cube of the dynamic contact angle is proportional to the capillary number Ca of the experiment, based on the viscosity and surface tension of the suspending liquid. These measurements are therefore consistent with the Cox-Voinov law, given by

Eq. 6 with a zero equilibrium contact angle, in agreement with the very small equilibrium angle of the suspensions on silicon wafers. A shift of the curves to higher values of the angle for identical values of Ca, is also observed, consistently with the viscosity increase due to addition of solid particles. However, this shift is found to be a function of particle size whereas the bulk viscosity of suspensions is not. The apparent viscosity of the suspensions during spreading, η_w, extracted from the experimental shifts is a function of both the particle size d_p and their volume fraction ϕ, decreasing down to the viscosity of the suspending liquid η_0 when the particle size is larger than around 150 µm.

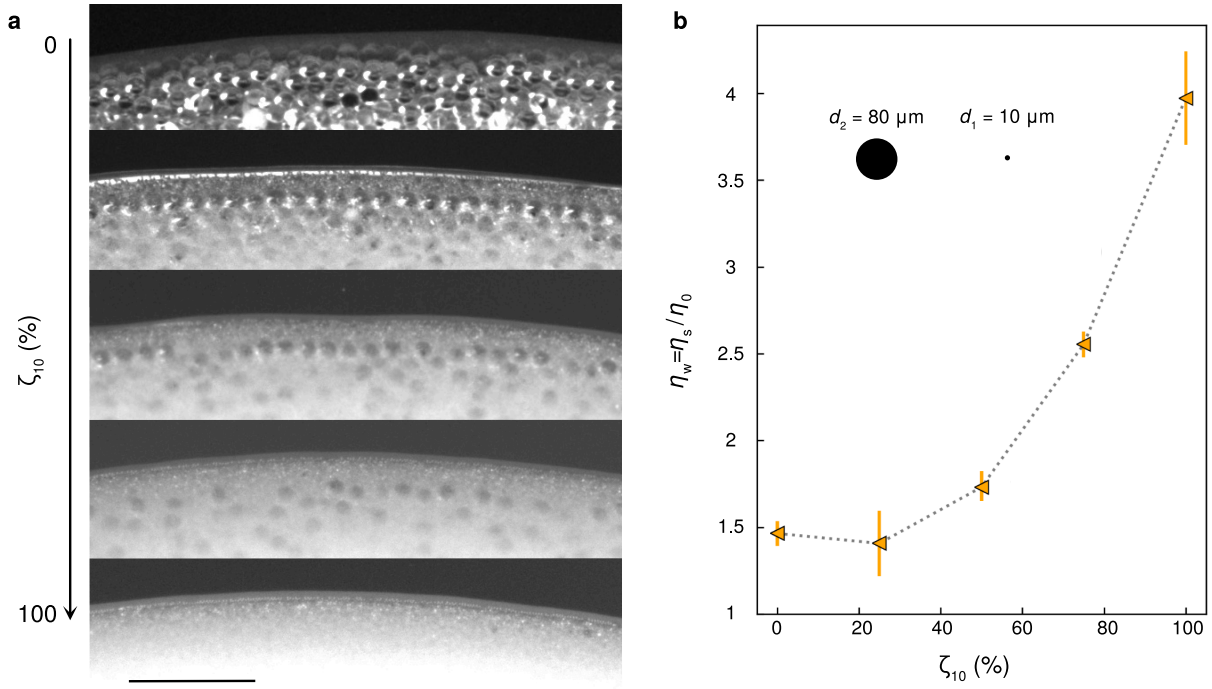

Figure 16: (a) Top views of the region near the contact line during the spreading of a bidipserse suspension of granular particles. The particles have diameter $d_1 = 10$ and $d_2 = 80$ µm. The fraction of 10-µm particles, $\zeta_{10} = 100 * \phi_{10}/\phi$ where ϕ_{10} is the volume fraction of small particles and ϕ the total volume fraction, increases from top to bottom. Scale bar: 500 µm. (b) Evolution of the viscosity ratio of granular suspensions $\eta_w = \eta_{s,w}/\eta_0$ where $\eta_{s,w}$ is the apparent viscosity of the suspension when spreading, as a function of the amount of small particles ζ_{10}. Adapted from Pelosse et al. [107].

A crucial observation reported by Zhao et al. [103] is that the region inside the droplet in the vicinity of the contact line is depleted in particles to a degree that depend on their size. With this observation in mind, Pelosse et al. [107] highlight the fact that the Cox-Voinov law

applies to contact angles that are measured at most a capillary length ℓ_c away from the contact line. They revisit a scaling analysis[108] that shows that the height of the liquid/gas interface in this domain ranges between 0 and a typical scale,

$$h^\star = (3Ca)^{1/3}\ell_c, \tag{23}$$

that is able to capture experimental data of the height of the interface at which the curvature changes sign in the case of a simple fluid. This length scale is a weak function of the capillary number: a tenfold increase of Ca increases $h^\star$ by a factor around 2 for a given liquid. It separates the droplet domain where the stress balance involves only capillarity and viscous dissipation from the region where gravity starts to influence the shape of the liquid/gas interface. As $10^{-3} \leq Ca \leq 10^{-2}$ in the reported experiments,[103,107] we have $250 \leq h^\star \leq 600$ µm. These values are of the same order of magnitude as the cut-off around 150 µm found by Zhao et al.[103]. They argue that only particles with sizes much smaller than $h^\star$ can affect the measurements of the dynamic contact angles, as they will be able to enter the viscous-capillary region and alter energy dissipation. This conclusion is supported by experiments[107] with bidisperse suspensions that show that the ability of small particles to move around larger ones and reach the visco-capillary region sets dissipation in the corner and in turn dictates the value of the dynamic contact angle (Fig. 16).

The theoretical description of the spreading of granular suspensions on a solid is still incomplete. A closer look at the contact line evidences that the first rows of particles experience strong confinement by both the liquid/gas and solid/liquid interfaces. The height of the interface in this region is of the order of a few particle sizes. As a result, particles arrange in a regular way, forming an ordered region that extends over a few particle diameters. Ordering under strong confinement between rigid walls leads to a decrease of the apparent viscosity of granular suspensions.[109] This effect is also expected to depend on inter-particulate friction and adhesion.[110,111] This element is absent of current modelling attempts and its contribu-

tion should be investigated in the future. Besides, particles hardly ever leave this region to go back to the bulk. Particle exchange is unidirectional, from the thicker parts of the droplet toward the contact line, as more particles can fit along the expanding perimeter of the spreading droplet. The dynamics of this region are at least qualitatively different from that of the bulk of the suspension.

Interestingly, the effect on wetting dynamics of particles ordering close to the contact line has been addressed with Brownian suspensions. For example, nanoparticles with diameters $d_p \sim 10$ nm promote the spreading of the liquid they are suspended in.[112–114] Spreading is enhanced because the particles form ordered layers in the vicinity of the contact line and modify the structural disjoining pressure. These systems are also sensitive to interactions between the substrate and the particles,[115] the liquid and the particles[116] and to the equilibrium wetting state. For example, theory predicts that the coupling between nanoparticles and the precursor film that precedes a droplet of completely wetting fluid should affect the dynamics and shape of the liquid.[117] To the best of our knowledge, these predictions have not been tested yet.

Similar finite-size effects as in suspensions are expected in emulsions. The spreading behaviour of emulsions has received little attention, although they are the workhorse fluids of many industries such as cosmetics, food and agriculture, either in manufacturing processes or final products. Besides, the resort to ink-jet printing in an ever broader range of applications suggests that this understanding will soon become crucial. Forester et al.[118] show that the radius of a droplet of water-in-silicone-oil emulsion spreading spontaneously on glass evolves as a power law of time with exponent 1/10, compatible with Tanner's law, given by Eq. 8, when the volume fraction of water is low. Spreading is slower for denser emulsions, and the spreading dynamics deviate more and more from Tanner's law at long times. The emulsion stops spreading when it contains more than 73% of water. The authors also show that the region next to the contact line is devoid of dispersed water droplets. Besides, the contact line exhibits an instability reminiscent of the fingering instability observed when a

surfactant solution spreads on a thin film of pure liquid.[119] The continuous phase of the emulsion used by Forester et al.[118] is a mixture of silicone oils loaded with surface-active molecules, and, as their liquids completely wet the substrate, it would be interesting to see whether their observations are compatible with a fingering instability of the precursor film.[6] Mohammad Karim and Kavehpour[120] study similar systems and they report that Tanner's law is valid over some range of their experiments. However, coarsening of the water droplets seems to affect their observations and makes it difficult to interpret the dynamics they report. Along the same line, Deblais et al.[121] demonstrate that the wettability of the solid by either the continuous or the dispersed phase must be taken into account in the description of the wetting of solids by emulsions. They also point out the need to account for yield stresses to shear appearing in dispersed systems, a point that is easier to explore in suspensions of soft particles as reviewed in the next section.

6.2 Flow dissipation in dispersed systems

Dispersed systems also display a large variety of responses to shear, which are expected to modify the dissipation in the shear flow compared to the simple liquid case described by Eq. 3. In the present Section, we focus on the changes of the shear flow due to finite-size effects in dispersed systems. A comprehensive study of the spreading dynamics of droplets of suspensions of soft particles was conducted in the case of dense suspensions of microgels by Martouzet et al.[122]. In these systems, hydrophilic polymer chains are swollen by water and arranged into a microstructure similar to that of a suspension with a characteristic size 1 μm.[123,124] As a first result, the microscopic cut-off length that sets the viscous dissipation is found to be equal to the microstructure lengthscale. Then, in the framework depicted in Fig. 2, the flow in the droplet is modified in three ways : a slip boundary condition at the liquid / solid interface, a yield stress for flow, and shear-thinning at large shear rates. We detail below their consequences on droplet spreading. First, on a smooth solid substrate,

a lubrication layer develops between the solid and the first layer of microgels[124,125] and translates into an effective slip length: it favors the droplet spreading at all times. This slip effect, however, disappears on a rough substrate with roughness of typical length equal to the microgel size. The yield stress and the shear-thinning effects operates at different stages of the drop spreading. The yield stress σ_y, of the order of tens of Pascals, becomes comparable to the shear stress at the later stage of the droplet spreading, and at some point, it stops the spreading before the thermodynamic contact angle θ_e is reached. Hence, the final contact angle θ_f depends on the spreading history since liquid was deposited. However, Martouzet et al.[122] derive a remarkably simple relationship between the final contact angle, the equilibrium contact angle and the ratio between the yield stress and the capillary pressure in the droplet at rest γ/R_f:

$$\cos\theta_f = \cos\theta_e + C\frac{\sigma_y}{\gamma/R_f} \tag{24}$$

where C is a constant that depends on the slip boundary condition. Beyond this analytical analysis, a numerical resolution of the full problem allows Martouzet et al.[122] to describe the measurement semi-quantitatively. Finally, at early stages where the spreading velocity is large, the shear rate is large enough so that the shear stress is larger than the yield stress everywhere in the droplet. The shear-thinning effect sets the wetting dynamics and can be described within the framework developed by Starov[96,126] for power-law fluids. Here, we choose not to review other non-Newtonian effects in droplets spreading and restrict to dispersed systems.

Altogether, and as mentioned in Section 6.1 for non-Brownian granular suspensions, the inter-particulate friction is expected to strongly affect the shear flow, not only close to the contact line where confinement and ordering occurs, but in the whole droplet where the rheological behavior of the suspension may be non-Newtonian. As an exemple, suspensions of frictionless particles often display counter-intuitive mechanical responses such as shear-thickening, while they are good candidate to probe the ordering under strong confinement at

the contact line in comparison to classical frictional[103,106,107] suspensions. Recent progress in the synthesis of model frictionless suspensions opens the ability to control interparticle interactions. The interplay between the confining Laplace pressure and the repulsive interparticle interaction may lead to interesting spreading dynamics. It will then be necessary to track the wetting dynamics both at the droplet scale and close to the contact line, at the particle scale.

7 Conclusion

In conclusion, the aim of the present article is to review recent experimental works on wetting dynamics, for which complexity arises from the nature either of the substrate or of the liquid. The guiding thread we have chosen is a departure of the dynamics from Cox-Voinov law. In the illustrations of this deviation given above, we have emphasised the key role of the different emerging length scales, either molecular, microscopic or mesoscopic that may result in a strong modification of the flow in the drop and/or the dissipation. In addition, transfers between surface and volume must be accounted for, as they modify the solid surface tension and thus the driving capillary term. These experimental works all point out the challenges in properly comparing the wetting dynamics data on complex systems or in complex situations with a reference experiment in order to separate the effects. As emphasised earlier, several effects are not fully understood yet, and studies on wetting dynamics have a bright future ahead of them.

Acknowledgement

The authors thank F. Boulogne, A. Deblais, J. Dervaux and F. Lequeux for discussions during the preparation of this review. M. R. is grateful to the Research School of Physics at the Australian National University (ANU) and to Centre National de la Recherche Scientifique (CNRS) for supporting his stay at the ANU during which this review was written through

a Stjepan Marčelja fellowship and the IEA grant "Coflact" respectively.

References

(1) de Gennes, P. G. Wetting : Statics and Dynamics. *Rev. Mod. Phys.* **1985**, *57*, 827–863.

(2) Bonn, D.; Eggers, J.; Indekeu, J.; Meunier, J.; Rolley, E. Wetting and Spreading. *Rev. Mod. Phys.* **2009**, *81*, 739–805.

(3) Snoeijer, J. H.; Andreotti, B. Moving Contact Lines: Scales, Regimes, and Dynamical Transitions. *Annu. Rev. Fluid Mech.* **2013**, *45*, 269–292.

(4) Sokuler, M.; Auernhammer, G. K.; Roth, M.; Liu, C.; Bonacurrso, E.; Butt, H.-J. The Softer the Better: Fast Condensation on Soft Surfaces. *Langmuir* **2010**, *26*, 1544–1547.

(5) Lee, H.; Alcaraz, M. L.; Rubner, M. F.; Cohen, R. E. Zwitter-Wettability and Antifogging Coatings with Frost-Resisting Capabilities. *ACS Nano* **2013**, *7*, 2172–2185.

(6) Bonn, D.; Eggers, J.; Indekeu, J.; Meunier, J.; Rolley, E. Wetting and spreading. *Rev. Mod. Phys.* **2009**, *81*, 739–805.

(7) Huh, C.; Scriven, L. E. Hydrodynamic Model of Steady Movement of a Solid/Liquid/Fluid Contact Line. *J. Colloid Interface Sci.* **1971**, *35*, 85–101.

(8) Voinov, O. V. Hydrodynamics of Wetting. *Fluid Dyn.* **1976**, *11*, 714–721.

(9) Cox, R. G. The dynamics of the spreading of liquids on a solid surface. Part 2. Surfactants. *J. Fluid Mech.* **1986**, *168*, 195.

(10) Snoeijer, J. H. Free-Surface Flows with Large Slopes: Beyond Lubrication Theory. *Phys. Fluids* **2006**, *18*, 021701.

(11) Fetzer, R.; Ramiasa, M.; Ralston, J. Dynamics of LiquidLiquid Displacement. *Langmuir* **2009**, *25*, 8069–8074.

(12) Cazabat, A. M.; Stuart, M. A. C. Dynamics of Wetting: Effects of Surface Roughness. *J. Phys. Chem.* **1986**, *90*, 5845–5849.

(13) Eddi, A.; Winkels, K. G.; Snoeijer, J. H. Short Time Dynamics of Viscous Drop Spreading. *Physics of Fluids* **2013**, *25*, 013102.

(14) McHale, G.; Newton, M. I.; Rowan, S. M.; Banerjee, M. The Spreading of Small Viscous Stripes of Oil. *J. Phys. D: Appl. Phys.* **1995**, *28*, 1925.

(15) Biance, A.; Clanet, C.; Quéré, D. First steps in the spreading of a liquid droplet -: art. no. 016301. *PHYSICAL REVIEW E* **2004**, *69*.

(16) Legendre, D.; Maglio, M. Numerical simulation of spreading drops. *Colloids and Surfaces A: Physicochemical and Engineering Aspects* **2013**, *432*, 29–37.

(17) Blake, T. D.; Haynes, J. M. Kinetics of Liquidliquid Displacement. *Journal of Colloid and Interface Science* **1969**, *30*, 421–423.

(18) Rolley, E.; Guthmann, C. Dynamics and Hysteresis of the Contact Line between Liquid Hydrogen and Cesium Substrates. *Phys. Rev. Lett.* **2007**, *98*, 166105.

(19) Prevost, A.; Rolley, E.; Guthmann, C. Thermally Activated Motion of the Contact Line of a Liquid 4 He Meniscus on a Cesium Substrate. *Physical Review Letters* **1999**, *83*, 348–351.

(20) Goossens, S.; Seveno, D.; Rioboo, R.; Vaillant, A.; Conti, J.; De Coninck, J. Can We Predict the Spreading of a Two-Liquid System from the Spreading of the Corresponding Liquid–Air Systems? *Langmuir* **2011**, *27*, 9866–9872.

(21) Petrov, P.; Petrov, I. A combined molecular-hydrodynamic approach to wetting kinetics. *Langmuir* **1992**, *8*, 1762–1767, _eprint: https://doi.org/10.1021/la00043a013.

(22) de Ruijter, M. J.; De Coninck, J.; Oshanin, G. Droplet spreading: Partial wetting regime revisited. *LANGMUIR* **1999**, *15*, 2209–2216, Num Pages: 8 Place: Washington Publisher: Amer Chemical Soc Web of Science ID: WOS:000079241200051.

(23) Blake, T.; Fernández-Toledano, J.-C.; De Coninck, J. A possible way to extract the dynamic contact angle at the molecular scale from that measured experimentally. *Journal of Colloid and Interface Science* **2023**, *629*, 660–669.

(24) Brochard-Wyart, F.; de Gennes, P. Dynamics of Partial Wetting. *Advances in Colloid and Interface Science* **1992**, *39*, 1–11.

(25) Petrov, J. G.; Ralston, J.; Schneemilch, M.; Hayes, R. A. Dynamics of Partial Wetting and Dewetting of an Amorphous Fluoropolymer by Pure Liquids. *Langmuir* **2003**, *19*, 2795–2801.

(26) Ramiasa, M.; Ralston, J.; Fetzer, R.; Sedev, R. Contact Line Friction in Liquid–Liquid Displacement on Hydrophobic Surfaces. *The Journal of Physical Chemistry C* **2011**, *115*, 24975–24986.

(27) Primkulov, B. K.; Lin, F.; Xu, Z. Microscale liquid-liquid displacement dynamics: Molecular kinetic or hydrodynamic control. *Colloids and Surfaces A: Physicochemical and Engineering Aspects* **2016**, *497*, 336–343.

(28) Duvivier, D.; Seveno, D.; Rioboo, R.; Blake, T. D.; De Coninck, J. Experimental Evidence of the Role of Viscosity in the Molecular Kinetic Theory of Dynamic Wetting. *Langmuir* **2011**, *27*, 13015–13021.

(29) Carlson, A.; Bellani, G.; Amberg, G. Universality in dynamic wetting dominated by contact line friction. *Phys. Rev. E* **2012**, *85*, 045302, arXiv:1111.1214 [physics].

(30) Wang, J.; Do-Quang, M.; Cannon, J. J.; Yue, F.; Suzuki, Y.; Amberg, G.; Shiomi, J. Surface structure determines dynamic wetting. *Sci Rep* **2015**, *5*, 8474.

(31) Lhermerout, R.; Davitt, K. Controlled defects to link wetting properties to surface heterogeneity. *Soft Matter* **2018**, *14*, 8643–8650.

(32) Perrin, H.; Lhermerout, R.; Davitt, K.; Rolley, E.; Andreotti, B. Thermally activated motion of a contact line over defects. *Soft Matter* **2018**, *14*, 1581–1595.

(33) Liu, C.; Bonaccurso, E.; Sokuler, M.; Auernhammer, G. K.; Butt, H.-J. Dynamic Wetting of Polyisoprene Melts: Influence of the End Group. *Langmuir* **2010**, *26*, 2544–2549.

(34) Schune, C.; Yonger, M.; Hanafi, M.; Thiel, J.; Guy, L.; Chaussée, T.; Lequeux, F.; Montes, H.; Verneuil, E. Morphology and Dynamics of Dense Nanometric Precursor Films of Polymer Melts. *Macromolecules* **2023**, acs.macromol.3c00554.

(35) Kavehpour, H. P.; Ovryn, B.; McKinley, G. H. Microscopic and Macroscopic Structure of the Precursor Layer in Spreading Viscous Drops. *Physical Review Letters* **2003**, *91*, 196104.

(36) Schune, C.; Yonger, M.; Hanafi, M.; Thiel, J.; Guy, L.; Chaussee, T.; Lequeux, F.; Montes, H.; Verneuil, E. Rouse 2D Diffusion of Polymer Chains in Low Density Precursor Films of Polybutadiene Melts. *Acs Macro Letters* **2020**, *9*, 843–848, Place: Washington Publisher: Amer Chemical Soc WOS:000542231400012.

(37) Brochard-Wyart, F.; di Meglio, J. M.; Quéré, D.; de Gennes, P. G. Spreading of Nonvolatile Liquids in a Continuum Picture. *Langmuir* **1991**, *7*, 335–338.

(38) Silberzan, P.; Léger, L. Evidence for a new spreading regime between partial and total wetting. *Physical Review Letters* **1991**, *66*, 185–188.

(39) Burlatsky, S. F.; Oshanin, G.; Cazabat, A. M.; Moreau, M.; Reinhardt, W. P. Spreading of a thin wetting film: Microscopic approach. *Physical Review E* **1996**, *54*, 3832–3845.

(40) Popescu, M. N.; Oshanin, G.; Dietrich, S.; Cazabat, A. M. Precursor films in wetting phenomena. *Journal of Physics Condensed Matter* **2012**, *24*, 1–51.

(41) Shull, K. Wetting Autophobicity of Polymer Melts. *Faraday Discussions* **1994**, *98*, 203–217, Place: Cambridge Publisher: Royal Soc Chemistry WOS:A1994RF56600017.

(42) Jopp, J.; Yerushalmi-Rozen, R. Autophobic Behavior of Polymers at the MeltElastomer Interface. *Macromolecules* **1999**, *32*, 7269–7275.

(43) Franiatte, S.; Tordjeman, P.; Ondarçuhu, T. Molecular Desorption by a Moving Contact Line. *Physical Review Letters* **2021**, *127*, 065501.

(44) Franiatte, S.; Tordjeman, P.; Ondarçuhu, T. Wetting at the Nanoscale: Molecular Mobility Induced by Contact Line Forces. *Langmuir* **2022**, *38*, 2614–2625.

(45) Naga, A.; Kaltbeitzel, A.; Wong, W. S. Y.; Hauer, L.; Butt, H.-J.; Vollmer, D. How a water drop removes a particle from a hydrophobic surface. *Soft Matter* **2021**, *17*, 1746–1755.

(46) Rondepierre, G.; De Soete, F.; Passade-Boupat, N.; Lequeux, F.; Talini, L.; Limat, L.; Verneuil, E. Dramatic Slowing Down of Oil/Water/Silica Contact Line Dynamics Driven by Cationic Surfactant Adsorption on the Solid. *Langmuir* **2021**, *37*, 1662–1673.

(47) Kekicheff, P.; Contal, C. Cationic-Surfactant-Coated Mica Surfaces below the Critical Micellar Concentration: 1. Patchy Structures As Revealed by Peak Force Tapping AFM Mode. *Langmuir* **2019**, *35*, 3087–3107, _eprint: https://doi.org/10.1021/acs.langmuir.8b03781.

(48) Schallamach, A. A theory of dynamic rubber friction. *Wear* **1963**, *6*, 375–382.

(49) Joanny, J.; Degennes, P. A Model for Contact-Angle Hysteresis. *JOURNAL OF*

CHEMICAL PHYSICS **1984**, *81*, 552–562, Num Pages: 11 Place: Melville Publisher: AIP Publishing Web of Science ID: WOS:A1984TA66100066.

(50) Singh, A. K.; Juvekar, V. A. Steady dynamic friction at elastomer–hard solid interface: A model based on population balance of bonds. *Soft Matter* **2011**, *7*, 10601.

(51) Li, X.; Bista, P.; Stetten, A. Z.; Bonart, H.; Schuer, M. T.; Hardt, S.; Bodziony, F.; Marschall, H.; Saal, A.; Deng, X.; Berger, R.; Weber, S. A. L.; Butt, H.-J. Spontaneous charging affects the motion of sliding drops. *NATURE PHYSICS* **2022**, *18*, 713+.

(52) Stetten, A. Z.; Golovko, D. S.; Weber, S. A. L.; Butt, H.-J. Slide electrification: charging of surfaces by moving water drops. *SOFT MATTER* **2019**, *15*, 8667–8679.

(53) Lester, G. R. Contact Angles of Liquids at Deformable Solid Surfaces. *J. Colloid Sci.* **1961**, *16*, 315–326.

(54) Carré, A.; Shanahan, M. E. R. Freinage Viscoélastique de l'étalement d'une Goutte. *C. R. Acad. Sci. Paris* **1993**, *317*, 1153–1158.

(55) Shanahan, M. E. R.; Carré, A. Anomalous Spreading of Liquid Drops on an Elastomeric Surface. *Langmuir* **1994**, *10*, 1647–1649.

(56) Long, D.; Ajdari, A.; Leibler, L. Static and Dynamic Wetting Properties of Thin Rubber Films. *Langmuir* **1996**, *12*, 5221–5230.

(57) Carré, A.; Shanahan, M. E. R. Viscoelastic Braking of a Running Drop. *Langmuir* **2001**, *17*, 2982–2985.

(58) Carre, A.; Shanahan, M. E. R. Direct Evidence for Viscosity-Independent Spreading on a Soft Solid. *Langmuir* **1995**, *11*, 24–26.

(59) Dervaux, J.; Roché, M.; Limat, L. Nonlinear Theory of Wetting on Deformable Substrates. *Soft Matter* **2020**, *16*, 5157–5176.

(60) Karpitschka, S.; Das, S.; van Gorcum, M.; Perrin, H.; Andreotti, B.; Snoeijer, J. H. Droplets Move over Viscoelastic Substrates by Surfing a Ridge. *Nat. Commun.* **2015**, *6*, 7891.

(61) Zhao, M.; Dervaux, J.; Narita, T.; Lequeux, F.; Limat, L.; Roché, M. Geometrical Control of Dissipation during the Spreading of Liquids on Soft Solids. *Proc. Nat. Acad. Sci. U.S.A.* **2018**, *115*, 1748–1753.

(62) van Gorcum, M.; Andreotti, B.; Snoeijer, J. H.; Karpitschka, S. Dynamic Solid Surface Tension Causes Droplet Pinning and Depinning. *Phys. Rev. Lett.* **2018**, *121*, 208003.

(63) van Gorcum, M.; Karpitschka, S.; Andreotti, B.; Snoeijer, J. H. Spreading on Viscoelastic Solids: Are Contact Angles Selected by Neumann's Law? *Soft Matter* **2020**, *16*, 1306–1322.

(64) Andreotti, B.; Snoeijer, J. H. Statics and Dynamics of Soft Wetting. *Annu. Rev. Fluid Mech.* **2020**, *52*, 285–308.

(65) Park, S. J.; B. Bostwick, J. B.; Andrade, V. D.; Je, J. H. Self-Spreading of the Wetting Ridge during Stick-Slip on a Viscoelastic Surface. *Soft Matter* **2017**, *13*, 8331–8336.

(66) Khattak, H. K.; Karpitschka, S.; Snoeijer, J. H.; Dalnoki-Veress, K. Direct Force Measurement of Microscopic Droplets Pulled along Soft Surfaces. *Nat. Commun.* **2022**, *13*, 4436.

(67) Snoeijer, J. H.; Rolley, E.; Andreotti, B. Paradox of Contact Angle Selection on Stretched Soft Solids. *Phys. Rev. Lett.* **2018**, *121*, 68003.

(68) Smith-Mannschott, K.; Xu, Q.; Heyden, S.; Bain, N.; Snoeijer, J. H.; Dufresne, E. R.; Style, R. W. Droplets Sit and Slide Anisotropically on Soft, Stretched Substrates. *Phys. Rev. Lett.* **2021**, *126*, 158004.

(69) Coux, M.; Kolinski, J. M. Surface Textures Suppress Viscoelastic Braking on Soft Substrates. *PNAS* **2020**, *117*, 32285–32292.

(70) Masurel, R.; Roché, M.; Limat, L.; Ionescu, I.; Dervaux, J. Elastocapillary Ridge as a Noninteger Disclination. *Phys. Rev. Lett.* **2019**, *122*, 248004.

(71) Pandey, A.; Andreotti, B.; Karpitschka, S.; van Zwieten, G. J.; van Brummelen, E. H.; Snoeijer, J. H. On the Singular Nature of the Elastocapillary Ridge. **2020**, 17.

(72) Oléron, M. Dynamic Wetting of Viscoelastic Substrates. Ph.D. thesis, Université de Paris, Paris, 2022.

(73) Amouroux, N.; Léger, L. Effect of Dangling Chains on Adhesion Hysteresis of Silicone Elastomers, Probed by JKR Test. *Langmuir* **2003**, *19*, 1396–1401.

(74) Cohen, C.; Restagno, F.; Poulard, C.; Léger, L. Incidence of the molecular organization on friction at soft polymer interfaces. *Soft Matter* **2011**, *7*, 8535.

(75) Hourlier-Fargette, A.; Antkowiak, A.; Chateauminois, A.; Neukirch, S. Role of Uncrosslinked Chains in Droplets Dynamics on Silicone Elastomers. *Soft Matter* **2017**, *13*, 3484–3491.

(76) Glover, J. D.; McLaughlin, C. E.; McFarland, M. K.; Pham, J. T. Extracting Uncrosslinked Material from Low Modulus Sylgard 184 and the Effect on Mechanical Properties. *J. Polym. Sci.* **2020**, *58*, 343–351.

(77) Tiwari, A.; Dorogin, L.; I. Bennett, A.; D. Schulze, K.; G. Sawyer, W.; Tahir, M.; Heinrich, G.; J. Persson, B. N. The Effect of Surface Roughness and Viscoelasticity on Rubber Adhesion. *Soft Matter* **2017**, *13*, 3602–3621.

(78) BROCHARDWYART, F.; DEGENNES, P.; LEGER, L.; MARCIANO, Y.; RAPHAEL, E. ADHESION PROMOTERS. *JOURNAL OF PHYSICAL CHEMISTRY* **1994**, *98*, 9405–9410.

(79) Ellul, M. D.; Gent, A. N. The role of molecular diffusion in the adhesion of elastomers. *Journal of Polymer Science: Polymer Physics Edition* **1984**, *22*, 1953–1968.

(80) Hourlier-Fargette, A.; Dervaux, J.; Antkowiak, A.; Neukirch, S. Extraction of Silicone Uncrosslinked Chains at Air–Water–Polydimethylsiloxane Triple Lines. *Langmuir* **2018**, *34*, 12244–12250.

(81) Wong, W. S. Y.; Hauer, L.; Naga, A.; Kaltbeitzel, A.; Baumli, P.; Berger, R.; d'Acunzi, M.; Vollmer, D.; Butt, H.-J. Adaptive Wetting of Polydimethylsiloxane. *Langmuir* **2020**, *36*, 7236–7245.

(82) Choi, G. Y.; Kim, S.; Ulman, A. Adhesion Hysteresis Studies of Extracted Poly(Dimethylsiloxane) Using Contact Mechanics. *Langmuir* **1997**, *13*, 6333–6338.

(83) Cai, Z.; Skabeev, A.; Morozova, S.; Pham, J. T. Fluid Separation and Network Deformation in Wetting of Soft and Swollen Surfaces. *Commun. Mater.* **2021**, *2*, 1–11.

(84) Hauer, L.; Cai, Z.; Skabeev, A.; Vollmer, D.; Pham, J. T. Phase Separation in Wetting Ridges of Sliding Drops on Soft and Swollen Surfaces. *Phys. Rev. Lett.* **2023**, *130*, 058205.

(85) Zhao, M.; Lequeux, F.; Narita, T.; Roché, M.; Limat, L.; Dervaux, J. Growth and Relaxation of a Ridge on a Soft Poroelastic Substrate. *Soft Matter* **2017**, *14*, 61–72.

(86) Xu, Q.; Wilen, L. A.; Jensen, K. E.; Style, R. W.; Dufresne, E. R. Viscoelastic and Poroelastic Relaxations of Soft Solid Surfaces. *Phys. Rev. Lett.* **2020**, *125*, 238002.

(87) Flapper, M. M.; Pandey, A.; Essink, M. H.; Van Brummelen, E. H.; Karpitschka, S.; Snoeijer, J. H. Reversal of Solvent Migration in Poroelastic Folds. *Phys. Rev. Lett.* **2023**, *130*, 228201.

(88) Dupas, J.; Verneuil, E.; Talini, L.; Lequeux, F.; Ramaioli, M.; Forny, L. DIFFUSION

AND EVAPORATION CONTROL THE SPREADING OF VOLATILE DROPLETS ONTO SOLUBLE FILMS. *Interfac Phenom Heat Transfer* **2013**, *1*, 231–243.

(89) Lequeux, F.; Talini, L.; Verneuil, E.; Delannoy, G.; Valois, P. Wetting of polymers by their solvents. *Eur. Phys. J. E* **2016**,

(90) Muralidhar, P.; Bonaccurso, E.; Auernhammer, G. K.; Butt, H.-J. Fast dynamic wetting of polymer surfaces by miscible and immiscible liquids. *Colloid Polym Sci* **2011**, *289*, 1609–1615.

(91) Dupas, J.; Verneuil, E.; Landeghem, M. V.; Bresson, B.; Forny, L.; Ramaioli, M.; Lequeux, F.; Talini, L. Glass Transition Accelerates the Spreading of Polar Solvents on a Soluble Polymer. *PHYSICAL REVIEW LETTERS* **2014**,

(92) Butt, H.-J.; Berger, R.; Steffen, W.; Vollmer, D.; Weber, S. A. L. Adaptive Wetting—Adaptation in Wetting. *Langmuir* **2018**, *34*, 11292–11304.

(93) Venzmer, J. Superspreading — 20 years of physicochemical research. *Current Opinion in Colloid & Interface Science* **2011**, *16*, 335–343.

(94) Nikolov, A.; Wasan, D. Current opinion in superspreading mechanisms. *Advances in Colloid and Interface Science* **2015**, *222*, 517–529.

(95) Wang, X.; Chen, L.; Bonaccurso, E.; Venzmer, J. Dynamic Wetting of Hydrophobic Polymers by Aqueous Surfactant and Superspreader Solutions. *Langmuir* **2013**, *29*, 14855–14864.

(96) Rafaı¨, S.; Bonn, D. Spreading of non-Newtonian fluids and surfactant solutions on solid surfaces. *Physica A: Statistical Mechanics and its Applications* **2005**, *358*, 58–67.

(97) Joanny, J. Kinetics of spreading of a liquid supporting a surfactant monolayer: Repulsive solid surfaces. *Journal of Colloid and Interface Science* **1989**, *128*, 407–415.

(98) Radulovic, J.; Sefiane, K.; Shanahan, M. E. R. Dynamics of Trisiloxane Wetting: Effects of Diffusion and Surface Hydrophobicity. *J. Phys. Chem. C* **2010**, *114*, 13620–13629.

(99) Karapetsas, G.; Craster, R. V.; Matar, O. K. On surfactant-enhanced spreading and superspreading of liquid drops on solid surfaces. *J. Fluid Mech.* **2011**, *670*, 5–37.

(100) Wei, H.-H. Marangoni-enhanced capillary wetting in surfactant-driven superspreading. *J. Fluid Mech.* **2018**, *855*, 181–209.

(101) Kovalchuk, N. M.; Simmons, M. J. Surfactant-mediated wetting and spreading: Recent advances and applications. *Current Opinion in Colloid & Interface Science* **2021**, *51*, 101375.

(102) Venzmer, J. Superspreading – Has the mystery been unraveled? *Advances in Colloid and Interface Science* **2021**, *288*, 102343.

(103) Zhao, M.; Oléron, M.; Pelosse, A.; Limat, L.; Guazzelli, É.; Roché, M. Spreading of Granular Suspensions on a Solid Surface. *Phys. Rev. Research* **2020**, *2*, 022031.

(104) Boyer, F.; Pouliquen, O.; Guazzelli, É. Dense Suspensions in Rotating-Rod Flows: Normal Stresses and Particle Migration. *J. Fluid Mech.* **2011**, *686*, 5–25.

(105) Palma, S.; Lhuissier, H. Dip-Coating with a Particulate Suspension. *J. Fluid Mech.* **2019**, *869*, R3.

(106) Guazzelli, É.; Pouliquen, O. Rheology of Dense Granular Suspensions. *J. Fluid Mech.* **2018**, *852*, P1.

(107) Pelosse, A.; Guazzelli, É.; Roché, M. Probing Dissipation in Spreading Drops with Granular Suspensions. *J. Fluid Mech.* **2023**, *955*, A7.

(108) Snoeijer, J. H.; Rio, E.; Le Grand, N.; Limat, L. Self-Similar Flow and Contact Line Geometry at the Rear of Cornered Drops. *Phys. Fluids* **2005**, *17*, 072101.

(109) Ramaswamy, M.; Lin, N. Y. C.; Leahy, B. D.; Ness, C.; Fiore, A. M.; Swan, J. W.; Cohen, I. How Confinement-Induced Structures Alter the Contribution of Hydrodynamic and Short-Ranged Repulsion Forces to the Viscosity of Colloidal Suspensions. *Phys. Rev. X* **2017**, *7*, 041005.

(110) Ness, C.; Seto, R.; Mari, R. The Physics of Dense Suspensions. *Annu. Rev. Condens. Matter Phys.* **2022**, *13*, 97–117.

(111) Lemaire, E.; Blanc, F.; Claudet, C.; Gallier, S.; Lobry, L.; Peters, F. Rheology of Non-Brownian Suspensions: A Rough Contact Story. *Rheol Acta* **2023**, *62*, 253–268.

(112) Wasan, D. T.; Nikolov, A. D. Spreading of Nanofluids on Solids. *Nature* **2003**, *423*, 156–159.

(113) Sefiane, K.; Skilling, J.; MacGillivray, J. Contact Line Motion and Dynamic Wetting of Nanofluid Solutions. *Advances in Colloid and Interface Science* **2008**, *138*, 101–120.

(114) Kondiparty, K.; Nikolov, A. D.; Wasan, D.; Liu, K.-L. Dynamic Spreading of Nanofluids on Solids. Part I: Experimental. *Langmuir* **2012**, *28*, 14618–14623.

(115) Huminic, G.; Huminic, A.; Dumitrache, F.; Fleaca, C.; Morjan, I. Experimental Study on Contact Angle of Water Based Si–C Nanofluid. *J. Mol. Liq.* **2021**, *332*, 115833.

(116) Han, J.; Kim, C. Spreading of a Suspension Drop on a Horizontal Surface. *Langmuir* **2012**, *28*, 2680–2689.

(117) Espín, L.; Kumar, S. Forced Spreading of Films and Droplets of Colloidal Suspensions. *J. Fluid Mech.* **2014**, *742*, 495–519.

(118) Forester, J. E.; Sunkel, J. M.; Berg, J. C. Spontaneous Spreading of Emulsions on Solid Surfaces: Morphology and Dynamics. *J. Appl. Polym. Sci.* **2001**, *81*, 1817–1825.

(119) Matar, O. K.; Craster, R. V. Dynamics of Surfactant-Assisted Spreading. *Soft Matter* **2009**, *5*, 3801.

(120) Mohammad Karim, A.; Kavehpour, H. P. Spreading of Emulsions on a Solid Substrate. *J Coat Technol Res* **2014**, *11*, 103–108.

(121) Deblais, A.; Harich, R.; Bonn, D.; Colin, A.; Kellay, H. Spreading of an Oil-in-Water Emulsion on a Glass Plate: Phase Inversion and Pattern Formation. *Langmuir* **2015**, *31*, 5971–5981.

(122) Martouzet, G.; Jørgensen, L.; Pelet, Y.; Biance, A.-L.; Barentin, C. Dynamic Arrest during the Spreading of a Yield Stress Fluid Drop. *Phys. Rev. Fluids* **2021**, *6*, 044006.

(123) Géraud, B.; Jørgensen, L.; Ybert, C.; Delanoë-Ayari, H.; Barentin, C. Structural and cooperative length scales in polymer gels. *The European Physical Journal E* **2017**, *40*, 5.

(124) Pemeja, J.; Geraud, B.; Barentin, C.; Le Merrer, M. Wall slip regimes in jammed suspensions of soft microgels. *PHYSICAL REVIEW FLUIDS* **2019**, *4*.

(125) Seth, J. R.; Locatelli-Champagne, C.; Monti, F.; Bonnecaze, R. T.; Cloitre, M. How do soft particle glasses yield and flow near solid surfaces? *SOFT MATTER* **2012**, *8*, 140–148.

(126) Starov, V.; Tyatyushkin, A.; Velarde, M.; Zhdanov, S. Spreading of non-Newtonian liquids over solid substrates. *Journal of Colloid and Interface Science* **2003**, *257*, 284–290.